Defense Threat Reduction Agency
8725 John J. Kingman Road, MS 6201
Fort Belvoir, VA 22060-6201

DTRA-TR-04-22

TECHNICAL REPORT

Integration of Enhanced Propagation, Environmental Variability, and Network Performance Models into the InfraMAP Software Toolkit.

Approved for public release; distribution is unlimited.

November 2007

DTRA01-00-C-0063

David Norris and Robert Gibson

Prepared by:
BBN Technologies
1300 North 17th Street
Suite 400
Arlington, VA 22209

DESTRUCTION NOTICE

FOR CLASSIFIED documents, follow the procedures in DoD 5550.22-M, National Industrial Security Program Operating Manual, Chapter 5, Section 7 (NISPOM) or DoD 5200.1-R, Information Security Program Regulation, Chapter 1X.

FOR UNCLASSIFIED limited documents, destroyed by any method that will prevent disclosure of contents or reconstruction of the document.

Retention of this document by DoD contractors is authorized in accordance with DoD 5220.22-M, Industrial Security Manual.

PLEASE NOTIFY THE DEFENSE THREAT REDUCTION AGENCY, ATTN: CST, 8725 JOHN J. KINGMAN ROAD, STOP-6201, FT BELVOIR, VA 22060-6201, IF YOUR ADDRESS IS INCORRECT, IF YOU WISH IT DELETED FROM THE DISTRIBUTION LIST, OR IF THE ADDRESSEE IS NO LONGER EMPLOYED BY YOUR ORGANIZATION.

DISTRIBUTION LIST UPDATE

This mailer is provided to enable DTRA to maintain current distribution lists for reports. (We would appreciate you providing the requested information.)

- ☐ Add the individual listed to your distribution list.
- ☐ Delete the cited organization/individual.
- ☐ Change of address.

Note:
Please return the mailing label from the document so that any additions, changes, corrections or deletions can be made easily. For distribution cancellation or more information call DTRA/CST (703) 767-4725.

NAME: _____

ORGANIZATION: _____

OLD ADDRESS	NEW ADDRESS
_____	_____
_____	_____
_____	_____

TELEPHONE NUMBER: ( ) _____

DTRA PUBLICATION NUMBER/TITLE	CHANGES/DELETIONS/ADDITONS, etc. *(Attach Sheet if more Space is Required)*
_____	_____
_____	_____
_____	_____

DTRA or other GOVERNMENT CONTRACT NUMBER: _____

CERTIFICATION of NEED-TO-KNOW BY GOVERNMENT SPONSOR (if other than DTRA):

SPONSORING ORGANIZATION: _____

CONTRACTING OFFICER or REPRESENTATIVE: _____

SIGNATURE: _____

DEFENSE THREAT REDUCTION AGENCY
ATTN: CST
8725 John J Kingman Road, MS 6201
Fort Belvoir, VA 22060-6201

DEFENSE THREAT REDUCTION AGENCY
ATTN:CST
8725 John J Kingman Road, MS 6201
Fort Belvoir, VA 22060-6201

REPORT DOCUMENTATION PAGE

Form Approved
OMB No. 0704-0188

1. AGENCY USE ONLY (Leave blank)	2. REPORT DATE	3. REPORT TYPE AND DATES COVERED
		Technical 000619 - 030619

4. TITLE AND SUBTITLE
Integration of Enhanced Propagation, Environmental Variability, and Network Performance Models into the InfraMAP Software Tool Kit.

5. FUNDING NUMBERS
PE - 463D
P - CD
TA - CD
WU - 02091

6. AUTHOR(S)
David E. Norris
Robert G. Gibson

7. PERFORMING ORGANIZATION NAME(S) AND ADDRESS(ES)
BBN Technologies
1300 North 17th Street
Arlington, VA 22209

8. PERFORMING ORGANIZATION REPORT NUMBER

9. SPONSORING/MONITORING AGENCY NAME(S) AND ADDRESS(ES)
Defense Threat Reduction Agency
8725 John J. Kingman Road, MS 6201
Fort Belvoir, VA 22060-6201
DSTN/Dainty

10. SPONSORING/MONITORING AGENCY REPORT NUMBER
DTRA-TR-04-22

11. SUPPLEMENTARY NOTES
This work was sponsored by the Defense Threat Reduction Agency under RDT&E RMSS Code B 463D D K540 CD CD 02091.

12a. DISTRIBUTION/AVAILABILITY STATEMENT
Approved for public release; distribution is unlimited

12b. DISTRIBUTION CODE

13. ABSTRACT *(Maximum 200 words)*

Enhancements to the infrasound software tool kit, InfraMAP, have been integrated in three main areas: propagation modeling, environmental variability modeling, and stochastic localization techniques. All new model functionality is included in a next-generation release of the tool kit. The modeling advances improve propagation predictions and understanding of environmental effects, and they have been used to evaluate the localization performance and confidence bounds of operational infrasonic networks.

New propagation modeling features include a high altitude, low frequency absorption model, a synthetic waveform generator from ray tracing, and an improved Parabolic Equation (PE) propagation algorithm. In environmental variability, a range-dependent spectral gravity wave model has been developed that generates wind perturbation fields for use in evaluating propagation variability. Finally, regional infrasound networks can be defined and used to compute source localizations and associated areas of uncertainty, based upon both measurement data and modeling results.

14. SUBJECT TERMS		15. NUMBER OF PAGES
Infrasound	Atmosphere	69
Long-Range Propagation	Test-Ban Verification	16. PRICE CODE

17. SECURITY CLASSIFICATION OF REPORT	18. SECURITY CLASSIFICATION OF THIS PAGE	19. SECURITY CLASSIFICATION OF ABSTRACT	20. LIMITATION OF ABSTRACT
UNCLASSIFIED	UNCLASSIFIED	UNCLASSIFIED	SAR

CONVERSION TABLE

Conversion Factors for U.S. Customary to metric (SI) units of measurement.

MULTIPLY →	BY →	→ TO GET
TO GET ←	BY ←	← DIVIDE

angstrom	1.000 000 x E -10	meters (m)
atmosphere (normal)	1.013 25 x E +2	kilo pascal (kPa)
bar	1.000 000 x E +2	kilo pascal (kPa)
barn	1.000 000 x E -28	meter^2 (m^2)
British thermal unit (thermochemical)	1.054 350 x E +3	joule (J)
calorie (thermochemical)	4.184 000	joule (J)
cal (thermochemical/cm^2)	4.184 000 x E -2	mega joule/m^2 (MJ/m^2)
curie	3.700 000 x E +1	*giga bacquerel (GBq)
degree (angle)	1.745 329 x E -2	radian (rad)
degree Fahrenheit	$t_k = (t°f + 459.67)/1.8$	degree kelvin (K)
electron volt	1.602 19 x E -19	joule (J)
erg	1.000 000 x E -7	joule (J)
erg/second	1.000 000 x E -7	watt (W)
foot	3.048 000 x E -1	meter (m)
foot-pound-force	1.355 818	joule (J)
gallon (U.S. liquid)	3.785 412 x E -3	meter^3 (m^3)
inch	2.540 000 x E -2	meter (m)
jerk	1.000 000 x E +9	joule (J)
joule/kilogram (J/kg) radiation dose absorbed	1.000 000	Gray (Gy)
kilotons	4.183	terajoules
kip (1000 lbf)	4.448 222 x E +3	newton (N)
kip/inch^2 (ksi)	6.894 757 x E +3	kilo pascal (kPa)
ktap	1.000 000 x E +2	newton-second/m^2 ($N-s/m^2$)
micron	1.000 000 x E -6	meter (m)
mil	2.540 000 x E -5	meter (m)
mile (international)	1.609 344 x E +3	meter (m)
ounce	2.834 952 x E -2	kilogram (kg)
pound-force (lbs avoirdupois)	4.448 222	newton (N)
pound-force inch	1.129 848 x E -1	newton-meter (N-m)
pound-force/inch	1.751 268 x E +2	newton/meter (N/m)
pound-force/foot^2	4.788 026 x E -2	kilo pascal (kPa)
pound-force/inch^2 (psi)	6.894 757	kilo pascal (kPa)
pound-mass (lbm avoirdupois)	4.535 924 x E -1	kilogram (kg)
pound-mass-foot^2 (moment of inertia)	4.214 011 x E -2	kilogram-meter^2 ($kg-m^2$)
pound-mass/foot^3	1.601 846 x E +1	kilogram-meter^3 (kg/m^3)
rad (radiation dose absorbed)	1.000 000 x E -2	**Gray (Gy)
roentgen	2.579 760 x E -4	coulomb/kilogram (C/kg)
shake	1.000 000 x E -8	second (s)
slug	1.459 390 x E +1	kilogram (kg)
torr (mm Hg, 0° C)	1.333 22 x E -1	kilo pascal (kPa)

*The bacquerel (Bq) is the SI unit of radioactivity; 1 Bq = 1 event/s.

**The Gray (GY) is the SI unit of absorbed radiation.

Table of Contents

Figures

Tables

Acknowledgements

Many people have assisted in the development of the multiple releases of InfraMAP over this and previous contracts, both through general discussions and by providing several of the base modeling capabilities contained in the software. In particular:

- Henry Bass of the National Center for Physical Acoustics, University of Mississippi, for feedback regarding model selection and use.
- Rod Whitaker and Doug ReVelle of Los Alamos National Laboratory (LANL) have provided many hours of discussion and direction on the modeling techniques and provided the WKB version of the normal mode code.
- Dean Clauter and Bob Blandford of the Air Force Technical Applications Center (AFTAC) provided guidance regarding the desired capabilities of the software and also provided historical data for validation purposes.
- Doug Drob of NRL's Upper Atmospheric Physics Branch provided advice and assistance regarding use of the HWM-93 and MSISE atmospheric models, available from the NRL web site, and also provided valuable insight regarding approaches to perturbation modeling of the propagation environment.
- Tom Georges of NOAA's Environmental Technology Laboratory provided the HARPA code, available from the NOAA/ETL ftp site, and a copy of the software documentation.

We would also like to acknowledge LANL and AFTAC for being beta test sites for the software.

Section 1
Summary

InfraMAP, *Infrasonic Modeling of Atmospheric Propagation*, is a software tool kit that has been developed for use by researchers and analysts active in the study of infrasonic propagation and monitoring. The original development effort is summarized in a previous report (Gibson and Norris 2002b). This report addresses enhancements that have been developed and integrated into new versions of the tool kit.

Enhancements to InfraMAP have been integrated in three main areas: propagation modeling, environmental variability modeling, and stochastic localization techniques. All new model functionality is included in a next-generation release of the tool kit. The modeling advances improve propagation predictions and understanding of environmental effects, and they have been used to evaluate the localization performance and confidence bounds of operational infrasonic networks.

Propagation modeling enhancements include a high altitude, low frequency absorption model, a synthetic waveform generator from ray tracing, and an improved Parabolic Equation (PE) propagation algorithm. In addition to higher fidelity predictions, the new functionality enables more flexibility in making model-to-model and model-to-data comparisons.

In environmental variability, a new environmental variability model has been integrated. Wind perturbations due to gravity waves are modeled in the spectral domain, and both height and range-dependent gravity wave dependencies are modeled. The spectral model is used to generate multiple realizations of the perturbed environment, which in turn are used to quantify the statistical variability of the propagation.

Finally, a network performance model has been added. The model supports definition of regional infrasound networks consisting of three of more sensor stations. Measurement data and modeling results across these networks are used to localize sources and compute associated areas of uncertainty. These capabilities allow for straightforward evaluation of the effects of measurement error, propagation uncertainty, and sensor configuration on source localization accuracy.

Section 2
Introduction

2.1 Background

Monitoring for nuclear explosions requires the ability to detect, localize, and discriminate nuclear events. For the Comprehensive Nuclear-Test-Ban Treaty (CTBT), this monitoring is being implemented over a global scale through installation of 60 infrasonic stations in the International Monitoring System (IMS). Compared to other, more mature monitoring technologies, infrasound has a greater number of unresolved issues, most of which involve the effects of atmospheric dynamics on propagation.

The standard method of infrasonic localization is based on taking measured back azimuths and arrival times and projecting them back to a source position. However, due to the temporal and spatial variability of the atmosphere, stable paths cannot be easily predicted for standard back-azimuth and time-of-arrival localization algorithms. It is generally anticipated that the ability to identify infrasound phases, and include the appropriate travel-time and bearing refraction corrections for each arrival into localization procedures, would dramatically improve localization performance. The degree to which these capabilities can be developed, and the specifics of how they should be used are major topics of research in the community.

Another infrasound issue of interest is waveform amplitude. Geometrical spreading, diffraction, scattering, and absorption all have potential effects on amplitude predictions. Predictions are necessary for determining detection thresholds and observability of individual phases. They can also be used in source discrimination, in particular for yield estimates.

Under a previous DTRA contract (DSWA01-97-C-0160), BBN has taken a significant step in addressing the needs within the infrasound monitoring community by developing the InfraMAP software tool kit. InfraMAP (*Infra*sonic *M*odeling of *A*tmospheric *P*ropagation) is composed of propagation models and upper-atmospheric characterizations, integrated to allow for user-friendly model execution and data visualization. It can be applied to predict travel times, bearings, and amplitudes from potential event locations worldwide. Temporal and spatial variability of the atmosphere is addressed by allowing range-dependent temperature and winds to be incorporated with the propagation models.

InfraMAP integrates three types of research-grade propagation models with two empirically based atmospheric models. The baseline set of acoustic propagation models consists of a three-dimensional ray theory model, a WKB version of the normal mode model, and a continuous-wave, two-dimensional parabolic equation model. The baseline empirical atmospheric models are the horizontal wind model [Hedin *et al.*, 1996] and the extended mass spectrometer-incoherent scatter radar temperature model [Picone *et al.*, 1997]. Wind, temperature, and densities are modeled from the surface into the thermosphere and include spatial, diurnal, and seasonal effects.

2.2 Purpose

Effective interpretation of infrasound signals in support of the Comprehensive Nuclear-Test-Ban Treaty is complicated by inherent spatial and temporal variability in the atmosphere. The evaluation of network performance for infrasound stations relies on propagation model predictions for specific event scenarios. The dynamic nature of the environment and its impact on the predictions must be an integral component of the network performance evaluation.

The motivation of this effort is to develop enhanced propagation models, environmental variability models, and stochastic localization techniques in support of an integrated network performance model for infrasound. The anticipated benefits to the nuclear explosion monitoring community are:

Improved modeling capabilities – Propagation modeling enhancement will improve the fidelity of the models, leading to more accurate estimates of location and yield. The model enhancements will also facilitate model-to-model and model-to-measurement comparisons, which will help define each model's performance and applicability.

Evaluation of IMS network – Network performance models will enable evaluation of the effectiveness of the IMS network for specified scenarios of interest.

Improved infrasound localization – Integration of environmental variability models into event-localization algorithms will improve event location and confidence bound estimates. The confidence bounds will be useful in determining the relative importance with which to treat the predictions.

Support of synergy-based localization – Confidence bounds attached to event-localization predictions will be useful as weighting factors in synergy-based localization algorithms that process predictions from multiple monitoring technologies.

2.3 Scope

This effort has been limited to integrating improved propagation models, variability models, and localization capabilities into new versions of the InfraMAP software tool kit. Specifically, the scope is limited to:

- Enhancing propagation modeling capabilities.
- Developing spectral environmental variability models.
- Developing network performance models that incorporate environmental variability.
- Performing model-to-model and model-to-measurement comparisons to validate models and define confidence levels.
- Integrating all model enhancements and increased functionality into a new release of the InfraMAP software tool kit.

2.4 Outline

This section provides an introduction to the research effort. The remainder of the report summarizes the technical work that has been performed. Section 3 addresses methods, assumptions, and procedures in the model development process. Section 4 discusses the results of the effort by describing the software functionality. Studies are also summarized that have been performed using the software. The report ends with conclusions and recommendations.

Section 3
Methods, Assumptions and Procedures

This section describes the approach to enhancing the InfraMAP capabilities. The propagation modeling enhancements are addressed first, followed by discussions of environmental variability and network performance. The section concludes with a summary of the software development methods.

3.1 Propagation Modeling

Propagation model enhancements were selected in order to support the project goals. They fall into two categories: improvements in sophistication and efficiency, and improvements to support model-to-model and model-to-measurement comparisons. Implementation of items in the first category will naturally lead to better predictions. That for the second category will facilitate definition of model confidence levels and aid in evaluation of model applicability.

Table 1 provides a summary of the strengths and weaknesses of the propagation models currently integrated into InfraMAP. This table was used to define the enhancements for integration into the three models, as detailed below.

Table 1. Strengths and weaknesses of baseline propagation models.

Propagation Model	Strengths	Weaknesses
Ray	• Prediction/Visualization of acoustic wave front trajectories • Three-dimensional domain • Accounts for moving medium • Accounts for range and azimuthal-dependent environment • Accounts for evolution of environment	• Poor amplitude predictions • Ray path approximation breaks down at low frequencies • High numerical load for many ray traces • No signal waveform predictions
Normal Mode	• Prediction of signal waveform • Accounts for source signal characteristics (in time domain)	• Two-dimensional domain (vertical slice) • Accounts for only range-independent environment • Potential for false reflections at upper boundary
Parabolic Equation (PE)	• Prediction/Visualization of amplitude field down range of source • Accounts for range-dependent environment • Accounts for source frequency • Accounts for acoustic ground impedance	• Two-dimensional domain (vertical slice) • Sensitivity to source-field characterization • Limited to continuous wave (CW) sources

3.1.1. Ray Model

The ray model integrated into InfraMAP is HARPA (*HA*miltonian *R*ay *P*ropagation in the *A*tmosphere) [Jones *et al.*, 1986]. It is defined in a three-dimensional domain by spherical coordinates. HARPA accounts for the moving medium and predicts ray path attenuation due to viscous and thermal losses. Interaction with the surface is handled with specular reflections.

Under BBN's efforts in CTBT hydroacoustic modeling, it was found that the difference in ray paths traced over an elliptical earth model versus a spherical earth model was non-trivial [Farrell and LePage, 1996]. The conclusion was that an elliptical earth model should be used for ray traces and ray-based travel-time grids, and the implementation of HARPA in InfraMAP has been enhanced by incorporating an elliptical earth model. This enhancement enables evaluation of ray sensitivity to the earth characterization.

Absorption can have a significant influence on detection of infrasound phases. For example, rays that sample the atmosphere above 120 km experience high levels of absorption and are generally not observed [Gibson *et al.*, 1998]. The absorption model used with HARPA in InfraMAP has been improved by incorporating the recent model developed by Sutherland and Bass [1996]. This absorption model is concluded to best account for the relevant physics of infrasound, as it was specifically developed with low-frequency propagation in mind.

To facilitate comparison of ray predictions to normal mode predictions, a signal phase model has been incorporated with HARPA in InfraMAP. The signal phase is predicted from a user-defined source function and a set of rays. Although absolute predictions of ray levels are of limited application, this technique has been used successfully in the ocean to associate ray arrivals with measured waveforms [Norris *et al.* 1996]. Each ray is used to superimpose, at the ray travel time, the source waveform weighted by the ray attenuation. Predicted phases of this type can be directly compared to normal mode predictions. In addition, multiple source functions can be used in comparisons with measurements to help quantify the source characteristics.

To further facilitate model-to-model comparisons, two environmental options have been incorporated in the ray model. The first option reduces the range-dependent environment to a range-independent one, i.e., a single environmental profile, specified at the source, receiver, or averaged along the source-receiver path. The second option reduces the time-dependent environment to a time-independent one, i.e., an environmental field frozen at a specified time. These comparison-based options are desired because range-dependent and time-dependent environments are not accounted for in the other propagation models in InfraMAP.

3.1.2. Parabolic Equation (PE) Model

Predicting the loss of an infrasonic signal as it propagates from source to receiver is important in the study of network performance. It helps determine the receiver station coverage and detection threshold for a given event scenario. It also aids in determining the observability of acoustic paths that sample the thermosphere, a region of high acoustic absorption. Thermospheric paths

are of particular interest because, when analyzed along with lower atmospheric paths, they can be used to estimate source position.

Loss predictions are made with the Parabolic Equation (PE) model. The PE model originally integrated into InfraMAP is a continuous-wave, finite-difference implementation with no absorption model [West *et al.*, 1992], and it can be applied to a vertical range-dependent slice of the atmosphere.

The PE model in InfraMAP has been improved by incorporating a more efficient, higher fidelity split-step algorithm [Jensen *et al.*, 1994]. In addition, an improved source field realization model has been integrated that more accurately models an omnidirectional point source. Both of these PE enhancements provide more accurate amplitude predictions.

The PE model has also been enhanced by adding an absorption model. In the thermospheric region above 100-130 km, absorption increases significantly. The main effect of the absorption is a reduction in acoustic energy from this region. The same absorption model used for the ray enhancements [Sutherland and Bass, 1996] has been integrated here, allowing for compatibility in comparisons.

Theoretical developments that enable travel time predictions of impulse sources from PE models have been evaluated in terms of feasibility and computational loading. Both the Time-Domain PE (TDPE) [Jensen *et al.*, 1994] and the Nonlinear Progressive wave Equation (NPE) [McDonald and Kuperman, 1987] have been identified as promising models for future development and application in the study of infrasonic propagation.

3.1.3. Normal Mode Model

The normal mode model in InfraMAP is a WKB approach [Dighe *et al.*, 1998; Hunter and Whitaker, 1997] of the normal mode model [Pierce and Kinney, 1976; Pierce *et al.*, 1973; Pierce and Posey, 1970]. It can be applied to a range-independent vertical slice of the atmosphere.

False reflections from the upper boundary of the normal mode model can appear in the waveform predictions, interfering with signal phase interpretation. An evaluation of the upper boundary has been made and optimal environmental boundary conditions have been identified and integrated in order to minimize false reflections.

3.2 Environmental Variability

Environmental properties vary in both space and time. Coherent spatial variability is observed at length scales from meters to thousands of kilometers, and temporal variability occurs over diurnal and seasonal time scales. The variability in wind and temperature makes modeling infrasound propagation difficult. Since the environment is dynamic and cannot be measured over the vast regions through which the infrasonic signals propagate, stochastic modeling methods are necessary to account for the environment's influence on propagation.

BBN has taken an initial step in this area by incorporating wind perturbation profiles in the InfraMAP ray calculations. The environmental perturbation fields are defined using a one-dimensional vertical wave number spectrum of the horizontal wind, and individual realizations of spatial fields are generated through a random-phase technique [Peitgen and Saupe, 1998]. A Monte Carlo simulation is executed where multiple rays are traced through the sum of mean and perturbed profiles. This simulation is used to estimate moments of travel-time and azimuthal deviation.

These modeling capabilities are a first step in addressing the variability issue. However, improving the stochastic environmental model is needed to more realistically represent the variability. The improvements are made by integrating a two-dimensional horizontal wave number spectrum model [Gardner, 1995, 1993]. This model captures the environmental variability associated with atmospheric gravity waves. Gravity waves are modeled because their spatial scales are of the same order as infrasonic wavelengths and thus they are suspected of having the greatest influence on propagation variability.

Ultimately, by better defining the spatial dependence and amplitudes of the environmental perturbations, better estimates of the stochastic properties of the propagation will be obtained. These estimates are an integral part of the network performance predictions, discussed in the next section.

3.3 Network Performance.

The CTBT monitoring network is designed to provide event-location estimates from observed infrasound signals at a set of monitoring stations. The sophistication of the propagation and environmental models, as well as the choice of localization algorithm, determines the accuracy of these estimates. A network performance model has been developed that incorporates enhanced propagation modeling and environmental variability. The performance model is based on predicted event locations and areas of uncertainty (AOU) for specified scenarios. The model includes comprehensive integration of the uncertainties across a network, which not only provides better performance predictions, but also helps quantify the influence of the propagation model enhancements and environmental variability.

The model uses a localization algorithm based on the Maximum Likelihood Estimator (MLE) approach (Kay, 1993). Other localization algorithms exist, but it has been determined that the performance difference between various algorithms is minimal. Back azimuth and arrival time measurements and associated uncertainties are used in the localizations. The uncertainties can include both measurement error and uncertainty associated with the propagation. Propagation variability due to the environment is also incorporated into the calculations, and estimates of event location and area of uncertainty (AOU) are accomplished.

3.4 Software Implementation.

The existing InfraMAP software tool kit serves as a development platform for model enhancement, creation, and evaluation. New functionality has been added to InfraMAP as the model development progresses, and incremental releases of InfraMAP software have been distributed to the user community.

In the development of the software, technical interaction with end users has provided valuable feedback with respect to refining the original design concepts. As an example, one user suggested the incorporation of the azimuthal equidistant projection to view topography and propagation predictions, as this projection is useful to quickly visualize range contours. The azimuthal equidistant projection is now an integrated InfraMAP option.

User support of the InfraMAP software tool kit has been provided in parallel with the other main tasks. This user support has served two purposes. First, full benefit of the tool kit has been ensured by offering technical help and customized routines for specific user needs. Second, relevant issues within the infrasonic community have been assimilated through technical interchange and user feedback. The feedback has been reviewed for unanticipated user needs, and, where appropriate, the focus of software development has been refined to provide maximum benefit and applicability to the infrasonic researcher and analyst.

Section 4
Results and Discussion

This section details the results and accomplishments that have been made under this contract. First, enhancements and new functionality to the InfraMAP software tool kit are reviewed. This area is presented with an initial overview, followed by detailed discussions in the areas of propagation modeling, environmental variability, and network performance. Second, references are given to the technical reports and presentations. The section concludes with a summary of the sensitivity and validation studies.

4.1 Overview of New InfraMAP Functionality.

The baseline InfraMAP software tool kit was released in 2000 [Gibson and Norris, 2002b]. Many new major and minor features have been added to the baseline release. They generally involve improving the graphical user interfaces (GUIs) or improving the model functionality. Table 2 provides a summary of new features added under this contract. Major additions to InfraMAP are discussed in this section. Full details concerning InfraMAP operation and options can be found in the latest User's Guide [Norris and Gibson, 2003].

Table 2. Overview of new InfraMAP functionality.

General Improvements	*Improved Model executables* - All model executables are compiled statically, which simplifies installation and improves performance
	Improved Print/Save form - Data from any figure can now be saved to MATLAB or text files
	Increased limit on number of Ray Trace step iterations per bounce - Prevents premature exit of ray tracing that can occur during perturbation runs
	New file interface supporting subdirectories for propagation run files
	Run Status Viewer – During propagation runs, the user can view the run status using the "Run Status" button on the Run/View form
	Run Log Viewer – Run messages are now printed to a log file instead of being displayed at the command line. The user can view the run log using the "View Run Log" button of the Run/View form

	Updated Ellipsoidal Earth Model – WGS84 standard. Spherical earth model radius set to average of ellipsoidal major and minor axis
	Extended Reverse Propagation Functionality – Option of specifying back azimuth when reverse propagation is selected
	New Coordinate Display Functionality – Option of specifying lat/lon coordinates in either decimal degrees or deg:min
Main Window Functionality Improvements	*New Map Overlay Functionality* – Option of overlaying map features on any lat/lon figure. Option of overlaying propagation scenario great circle path on any lat/lon figure
	Easier Cross–Application settings transfer – New option for transferring Propagation Scenario form data to Propagation Model form
	New variable options for MSIS - Molecular weight and specific heat ratio computed from MSIS can be displayed in the View Environment form
Ray Model/Interface Improvements	*Improved Eigenray finder* - Two passes over initial search over fan of rays now includes correction for azimuthal deviation, reducing the probability of missing candidate eigenrays
	New Ray Synthesis Functionality – Ray path predictions can now be coupled with a source waveform to predict a receiver envelope that includes propagation losses due to spreading and atmospheric absorption. The user can select from a Pierce blast wave pulse, a variable width Gaussian pulse or a user-defined source waveform
	Sutherland and Bass Absorption Model – Sutherland and Bass's atmospheric absorption model can now be included in ray synthesis waveform predictions
	Range Independent HWM/MSIS Option
	Ellipsoidal Earth Option for the Ray Model
Normal Mode Model/Interface Improvements	*Independent Specification of number of points used in upper/lower duct dispersion curve solutions*
	Specification of time window for averaging of normal mode model waveforms
	New upper boundary condition for normal mode code that better models receiver amplitudes for thermospheric arrivals

	Auto scaling option for amplitude axis of normal mode waveform plots
PE Model/Interface Improvements	*Improved upper boundary condition (absorption layer) that eliminates false reflections*
	Range-independent environmental options similar to that for ray and normal mode models
	Sutherland and Bass Absorption Model – Sutherland and Bass's atmospheric absorption model can now be included in Parabolic Equation propagation predictions
	ON/OFF button for Time Evolution of Environment in PE Model
	New Split-Step Algorithm and Source Specification
	New PE Model Display Option – User specification of amplitude reference distance
	Separate steps/wavelength inputs for height and range
Propagation Variability Improvements	*New Gravity wave spectral model for wind perturbation*
	New range-dependent specification of perturbation field
	New plots for Monte Carlo simulation that show path of reference ray and perturbed rays in both vertical and horizontal plane
	New option to fix range of perturbed ray tracing - This option is useful if perturbed rays deviate excessively from reference ray.
Network Performance Improvements	*New Source Localization form that supports calculation of source location and area of uncertainty based on input azimuth and travel time data across selected network*
	Improved Station Location and Station Network forms
	Updates to infrasound station database to include more recent locations and names
	Comprehensive updates to IMS and prototype infrasound station locations

4.2 Propagation Modeling Enhancements.

The three propagation models (ray trace, normal mode, PE) have a variety of capabilities and environmental interface options. They are summarized in Table 3. The PE and ray trace models

are range-dependent models, while the normal mode model only propagates through a range-independent environment. Three-dimensional effects, such as azimuthal deviation, are only predicted using ray tracing. The normal mode model produces waveform predictions, and the ray trace model can be used to generate synthetic waveforms based upon an assumed source function. Details concerning the propagation modeling are given in the following subsections.

Table 3. Summary of propagation capabilities and environmental interface options.

Predictive Capabilities	Travel Time	Azimuth Deviation	Waveform	Absorption	Environemnt Options	User-defined Profiles	HWM/MSIS Range Dep.	HWM/MSIS Range Indep.	HWM/MSIS Freeze Time	Earth Curvature
Ray Tracing (3-D) - *HARPA (NOAA)* - *Geometrical acoustics*	YES	YES	synthetic	YES		YES	YES	YES	YES	YES
Normal Modes (WKB) - *Modified Pierce code* - *Multi-mode summation*	YES		YES			YES		YES		
Parabolic Equation (2-D) - *Split-step PE* - *Range-marching*				YES		YES	YES	YES	YES	

4.2.1 Ray Tracing Model.

The 3-D ray tracing code HARPA (Hamiltonian Ray Tracing Program for Acoustic Waves in the Atmosphere) was developed at NOAA and provides ray predictions through an inhomogeneous three-dimensional representation of the atmosphere [Jones *et al.*, 1986]. The model accounts for vertical and horizontal refraction as well as horizontal translation of the ray path due to the moving medium. Horizontal refraction and translation effects are important in that they can cause significant azimuth biases in the propagation path. HARPA output includes azimuth and elevation angle, travel time, and azimuthal deviation at each point along a ray path. The ray tracing technique is capable of stepping either forward from a source or backward from a receiver. In InfraMAP, HARPA has been integrated with an eigenray finder, so that rays can be identified that connect a source and a receiver to within a given miss distance.

The ray tracing model has been enhanced with a new version of the eigenray finder. The eigenray algorithm starts by shooting a fan of rays over elevation angle along an azimuth directed toward the receiver. A second fan of rays is computed in the new version. The fan is identical except that the azimuth for each ray is corrected for azimuthal deviation. The

correction improves the robustness of the algorithm in scenarios with long ranges or strong crosswinds. The miss distance to the receiver is computed for the rays in the second fan, and rays that correspond to local minima in the miss distance are identified. These rays are then used as candidate eigenrays. Each candidate ray is perturbed in both azimuth and elevation angle until a minimum miss distance to the receiver is found. The ray is identified as an eigenray if the miss distance falls within the user specified limits.

A synthetic waveform option has also been added for use with the ray trace model. The source waveform is first selected, which can be defined as blast wave, Gaussian waveform, or user-defined waveform. The blast wave is computed from the formulation used in InfraMAP's normal mode code (Pierce and Posey, 1970). Figure 1 shows a blast wave for a 1 kT source on the ground.

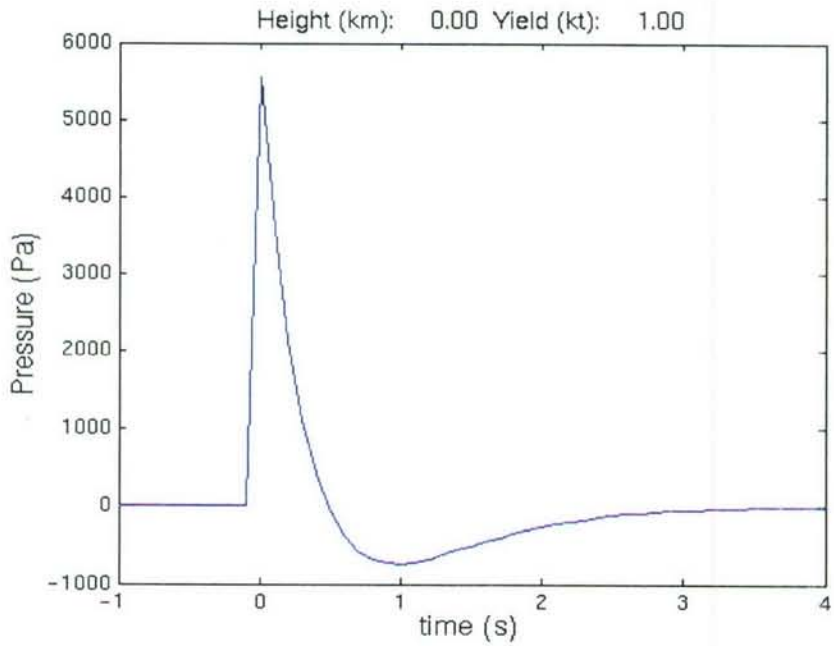

Figure 1. Blast waveform model for a 1 kT source on the ground [Pierce and Posey, 1970].

Once the source waveform is selected, the synthetic waveform is computed by convolving the source waveform with weighted impulse functions at the arrival times of the selected rays. The impulse functions are weighted by the attenuation loss calculated over each ray. Figure 2 provides a graphical representation of the waveform synthesis process.

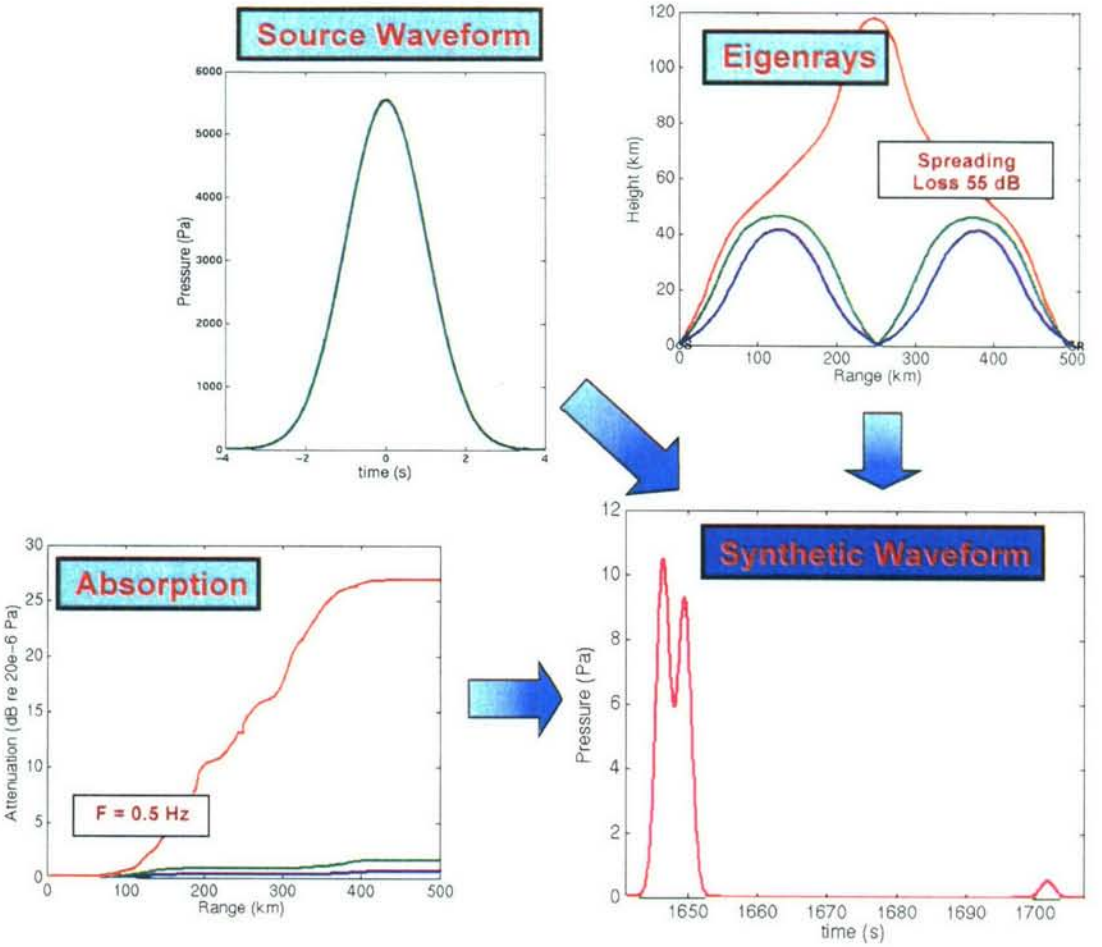

Figure 2. Graphical flow diagram depicting synthetic waveform process.

4.2.2 Normal Mode Model.

A version of Pierce's normal mode code, modified for prediction of lower-yield nuclear events, has been developed by Los Alamos National Laboratory [Dighe *et al.*, 1998; Hunter and Whitaker, 1997]. The model uses the Wentzel-Kramer-Brillouin (WKB) method to calculate a dispersion curve, which in turn is used to calculate a received waveform at a given range and azimuth. The waveform is computed from the summed set of modal solutions. Only range-independent environments are supported, which can be based on source location, receiver location, or from averaged values along the entire propagation path. The special case of dual-duct propagation is identified and automatically processed, in which case the full waveform solution is the sum of the upper and lower duct solutions.

The normal mode model uses an isothermal half-space as an upper boundary condition. In working with Los Alamos National Laboratory (Rod Whitaker), amplitude predictions for thermospheric arrivals were observed to be too strong when compared to observations, and energy returned from the upper boundary conditions was identified to contribute to this problem. As a result, the isothermal half-space has been modified to reduce the strength of thermospheric arrivals.

4.2.3 Parabolic Equation Model.

The Parabolic Equation (PE) algorithm steps forward from a source, characterized by a starter field, and calculates an amplitude field in height and range at a single frequency. The atmosphere is defined at each range step and can be range-dependent. The baseline PE version used a finite-difference approach. The model has been upgraded by integrating a split-step Fourier algorithm approach [Jensen *et al.*, 1994]. The new version is computationally more efficient and more accurately models the source function. The upper boundary condition has been modified to eliminate false reflections that could appear in the baseline version.

A new environmental interface option has also been added to the PE model. PE predictions can be made through an environment that is evolving in time. A mean signal velocity must be defined for a given scenario, and this is used to update the "local" time at each PE marching solution range. This time is then used in the retrieval of the HWM/MSIS environmental data, thus incorporating the environmental time evolution in the propagation predictions.

4.2.4 Absorption

An acoustic absorption model has been integrated for use with the PE and ray tracing models to improve the accuracy of the amplitude predictions. The absorption model chosen was developed specifically for use with low frequencies and altitudes up to 160 km [Sutherland and Bass, 1996]. It includes the contributions from both classical (translation and diffusion) and relaxation (rotation and vibration) losses. The model computes absorption using vertical profiles of temperature, pressure, and the concentration of gases that make up the air. All of these input variables are obtained from the MSISE-90 model (Picone et al., 1997). Figure 3 gives an example of the MSIS gas densities that are used for computing absorption. See Section 4.6.2 for example absorption coefficient profiles.

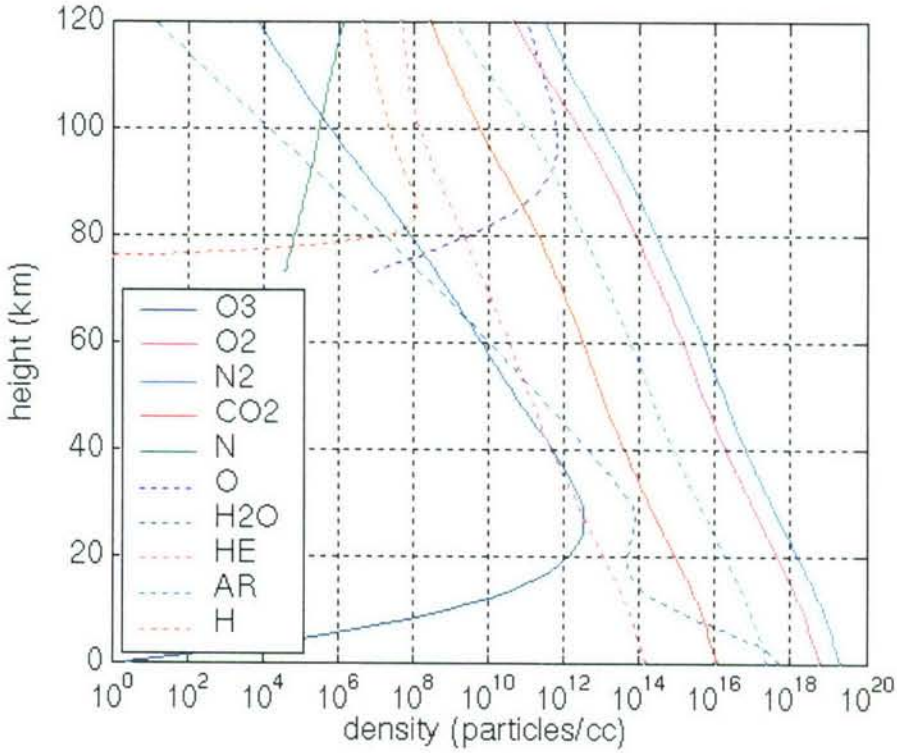

Figure 3. Example profiles of MSISE-90 gas densities used in the absorption model.

4.3 Environmental Variability Enhancements

The baseline environmental variability model in InfraMAP uses a power-law wind perturbation spectrum, and it provides realizations of wind perturbation profiles. This spectrum is applicable for small-scale turbulence, even though atmospheric turbulence covers a wide spectrum of spatial scales. The dominant source of variability affecting infrasonic propagation is believed to result from gravity waves. Gravity waves result from oscillations of air parcels displaced by buoyancy and restored by gravity. The oscillations have time scales ranging from minutes to tens of hours. Vertical length scales of gravity waves are in the range of 0.1 to 10 km, and horizontal scales can span from 100 to 10,000 km.

A significant body of research has been carried out to define the spectral character of gravity waves. The spectral model of Gardner [Gardner 1995, 1993] has been selected for integration into the environmental variability module. This model is based on scale-independent diffusive filtering theory. A source spectrum is defined near the ground. As the spectrum is propagated up in height, attenuation is modeled by introduction of diffusive damping. The key spectral properties are:

- increase in energy with height
- shift towards larger length scales with height
- attenuation of smaller length scales with height

The Gardner Spectral model is evaluated at four discrete heights, as shown in Figure 4. These heights capture the dominant gravity wave variability from the troposphere up to the lower thermosphere. Gravity waves are not fully developed below the troposphere. In the thermosphere, diffusion increases dramatically and gravity waves are damped out. In the figure, the predicted standard deviations of the wind perturbations are listed alongside the spectral heights.

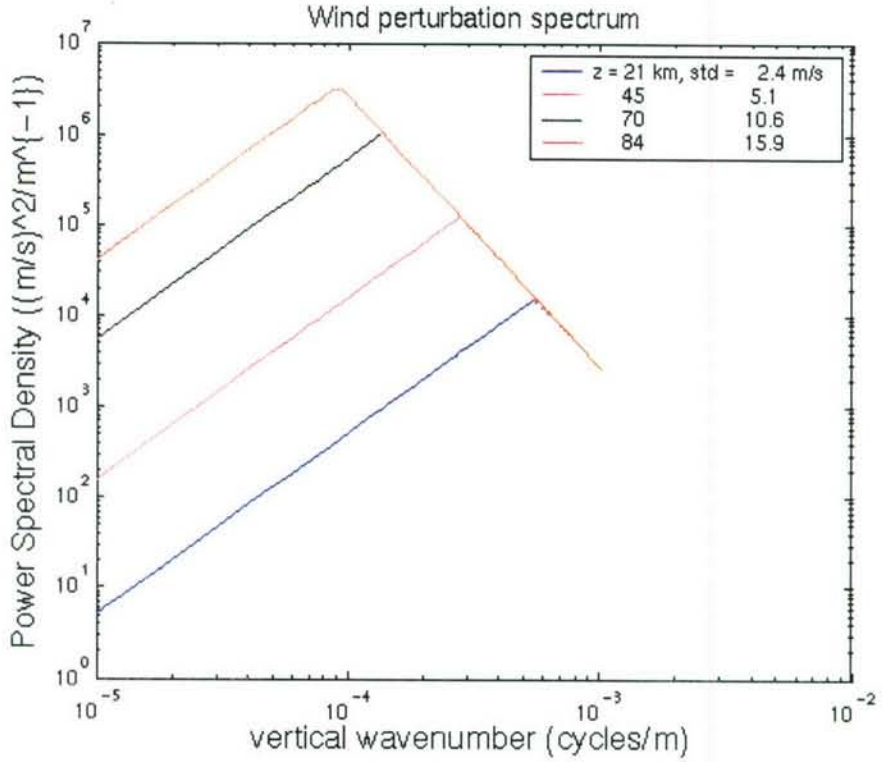

Figure 4. Wind perturbation spectra from Gardner's gravity wave model.

Fourier inversion using random phase is applied to the spectra to generate realizations of wind perturbation profiles. A wind perturbation profile is generated for each of the five spectra. A composite profile is then computed by shading each profile spatially with a Gaussian filter and then summing them together, where Gaussian filter half-power points are set to the midpoint between each of the spectral heights. To model range-dependent variability, a dominant horizontal length scale is defined, and Gaussian weighting functions are used to combine the wind perturbation profiles. Figure 5 gives an example realization of a wind perturbation field generated from the gravity wave spectral mode using a horizontal correlation length of 500 km. See Section 4.6.4 for an example application of using the gravity wave model to compute propagation variability.

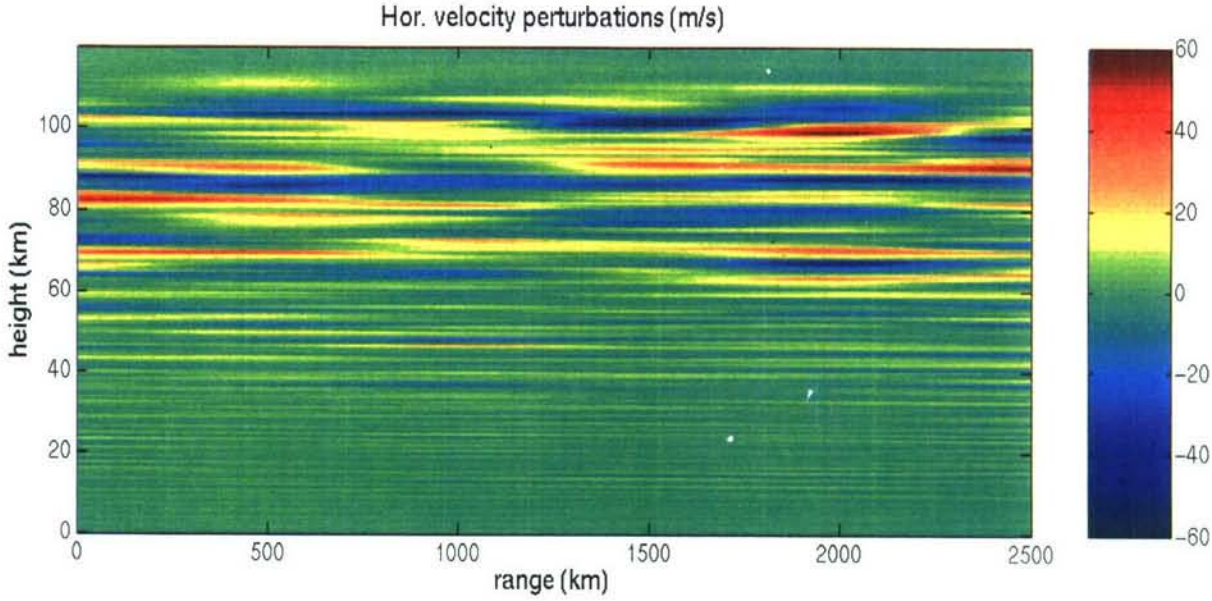

Figure 5. Example realization of range-dependent wind perturbation field.

4.4 Network Performance.

The enhancements to InfraMAP include the capability to evaluate network performance. This capability is accessed through use of a new Source Localization form (Figure 6), and it enables the localization of events based upon measurement data and modeling results. See Section 4.7.4 for an example application of the network performance capabilities.

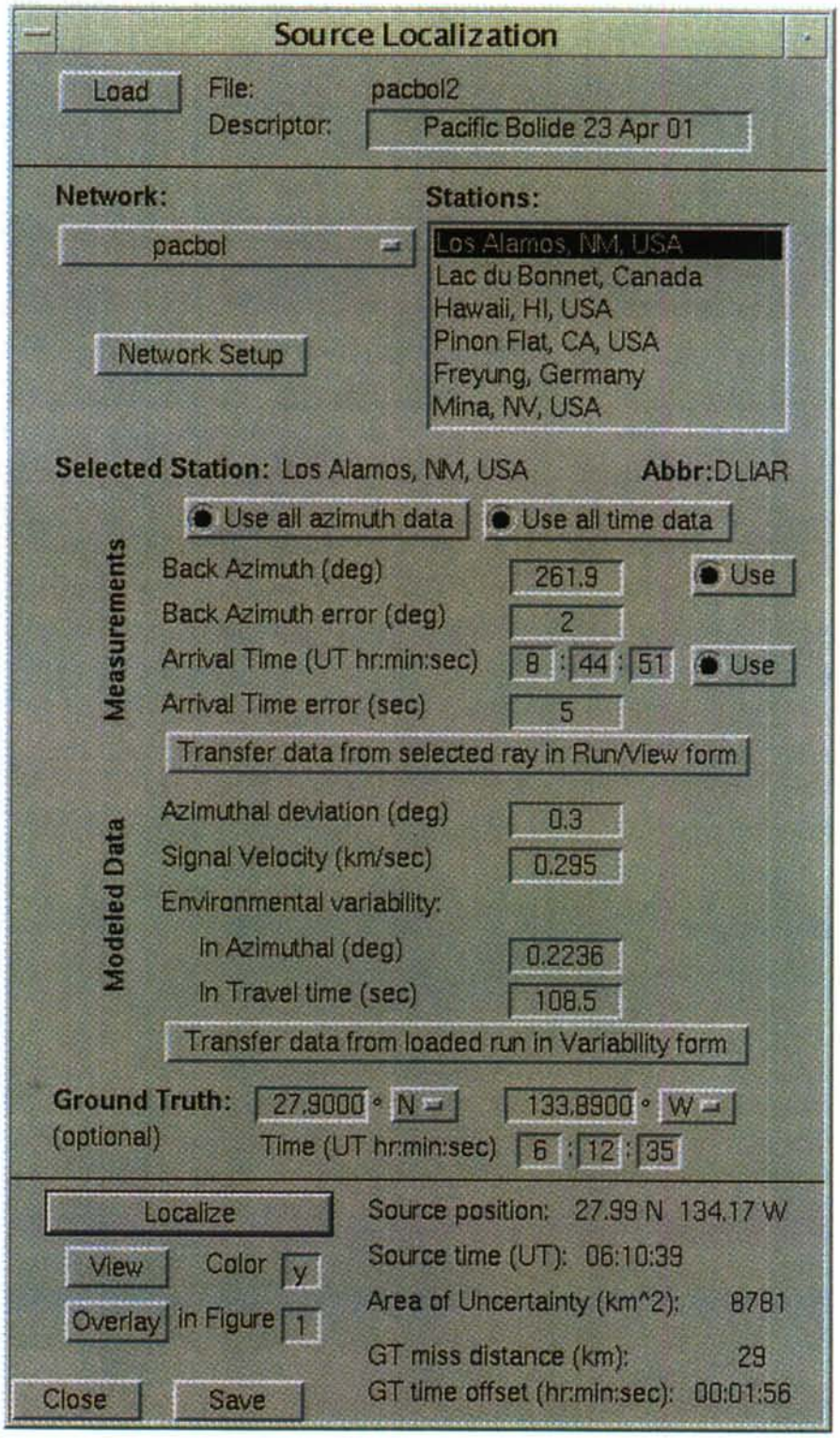

Figure 6. Source Localization form that provides the interface to the network performance capabilities.

The localization algorithm is a Maximum Likelihood Estimator (MLE) implementation (Kay, 1993) in geophysical coordinates (Perl, 1981). The inputs to the MLE algorithm are a set of back azimuth and arrival time measurements and associated uncertainties from a finite number of spatially separated sensors. The uncertainties can include both measurement error and uncertainty associated with the propagation, as discussed in later sections. The state of interest is positioned in spherical coordinates (lat, lon) and origin time. The basic algorithm can be applied to subsets of the measurements, but note that the state vector does not include an origin time if only azimuthal information is used.

The measurement equation relates the measurements to the state. For azimuth, it is determined directly from the spherical geometry. The arrival time is related to the state by defining the average sound velocity, or *signal velocity*, along the propagation path, where the signal velocity is defined as the total great circle range divided by the travel time (measured arrival time minus origin time). Because the measurement equation is nonlinear, it must be expanded around a reference state and a Jacobian matrix computed. The Jacobian matrix is the partial derivative of the measurement equation with respect to the state variables.

The Jacobian matrix and measurement inputs are combined to form the Fisher information matrix, from which an unbiased estimate of the state can be made. Implicit in this estimate is the assumption that the uncertainties can be represented as zero mean Gaussian distributions. Depending on the accuracy of the initial reference state, it may be necessary to iterate until convergence is reached. A covariance matrix that specifies the uncertainty in the state estimate is also computed. It is a non-trivial but straightforward analytic exercise to map the covariance matrix into an uncertainty ellipse over a specified confidence bound [Farrell and LePage, 1996]. The confidence bound is usually chosen as plus/minus 2 standard deviations or 95%.

4.5 Reports to the Research Community.

Under this contract, BBN participated in the 22nd Annual Seismic Research Symposium [Gibson and Norris, 2000], 23rd Seismic Research Review [Norris and Gibson, 2001a], and 24th Seismic Research Review [Norris and Gibson, 2002a]. The participation included submission of papers for the proceedings, presentation of posters, and attendance at meeting activities.

BBN also has given technical reports in several other meetings. We presented research on infrasonic propagation from bolides at the LANL sponsored Superbolide Workshop [Norris *et al.*, 2001]. Our work on bolide propagation, including an analysis of elevated ducts, was given at the Infrasound Technology Workshop Kauila-Kona [Norris and Gibson, 2001b]. At the Infrasound Technology Workshop in De Bilt, we presented work on environmental variability effects [Gibson and Norris, 2002a]. Finally, our work on localization accuracy of the Pacific bolide was given during a special session on infrasound at the Acoustical Society of America meeting in Cancun [Norris and Gibson, 2002b].

4.6 Sensitivity Analyses.

Several sensitivity studies have been carried out under this contract. They have focused on applying the enhanced environmental and propagation capabilities to evaluate the effect of various environmental variables and conditions on infrasonic propagation.

4.6.1 Environmental Time Evolution.

A new feature in InfraMAP is the ability to allow for time evolution of the environment during a propagation run. This capability can be used with both ray tracing and PE codes. Alternatively, a user can freeze the time evolution at a fixed time (e.g., the event time). With time evolution enabled, the climatological profiles at a point along the propagation path are determined based on the origin time plus the elapsed time of the ray (or of the step along the PE slice). In a "frozen" time scenario, all climatological profiles are referenced to the same time.

A study was conducted on the significance of the diurnal effect on propagation by comparing ray and PE results both with and without time evolution enabled. In this study, the source event time was used in the case where time evolution was frozen. The HWM-93 and MSISE-90 climatologies were used to model diurnal effects. Because diurnal effects are most prevalent in the thermosphere, thermospheric paths were selected for analysis.

The scenario chosen for modeling is as follows. The source was located in central Asia, at 78° E, 50.5° N. The source time was 15-Sept (Day 258) at 10 UT. A propagation path of 2500 km to the north was modeled using both eigenrays and a PE solution. The path corresponds to a travel time of approximately three hours (10 - 13 UT). Based on the climatology, both the zonal and meridional winds shift direction in the thermosphere during this time window, over the region of infrasound propagation. The nominal propagation path is shown in Figure 7.

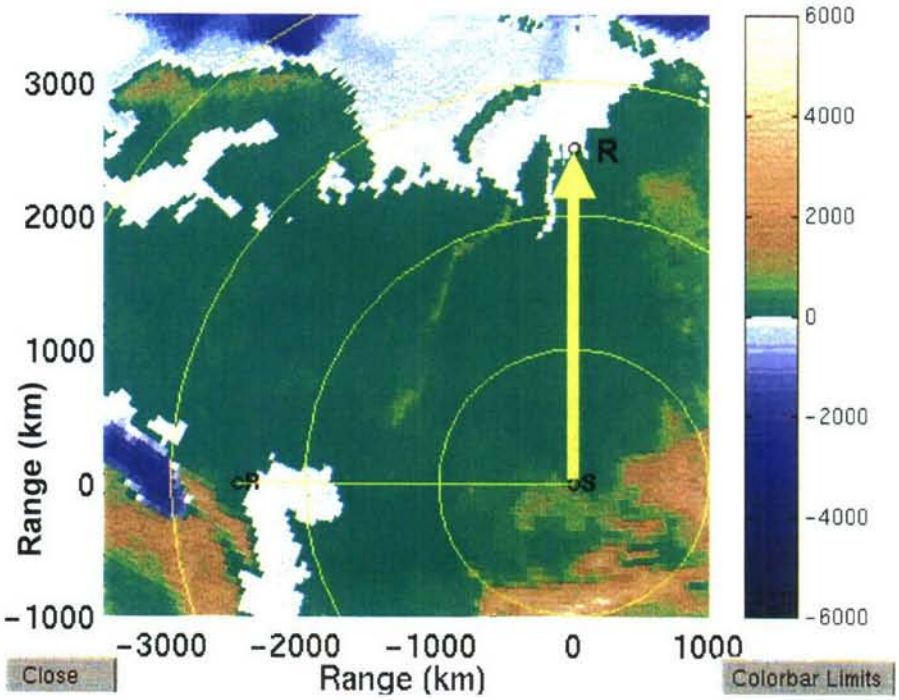

Figure 7. Nominal propagation path (arrow) for time evolution sensitivity study.

The effective sound speed in the direction of propagation along the great circle path is shown in Figure 8. The panel on the left shows the evolving environment, and the panel on the right shows the frozen environment. Based on the climatology, time evolution increases the turning heights of infrasound in the thermospheric region.

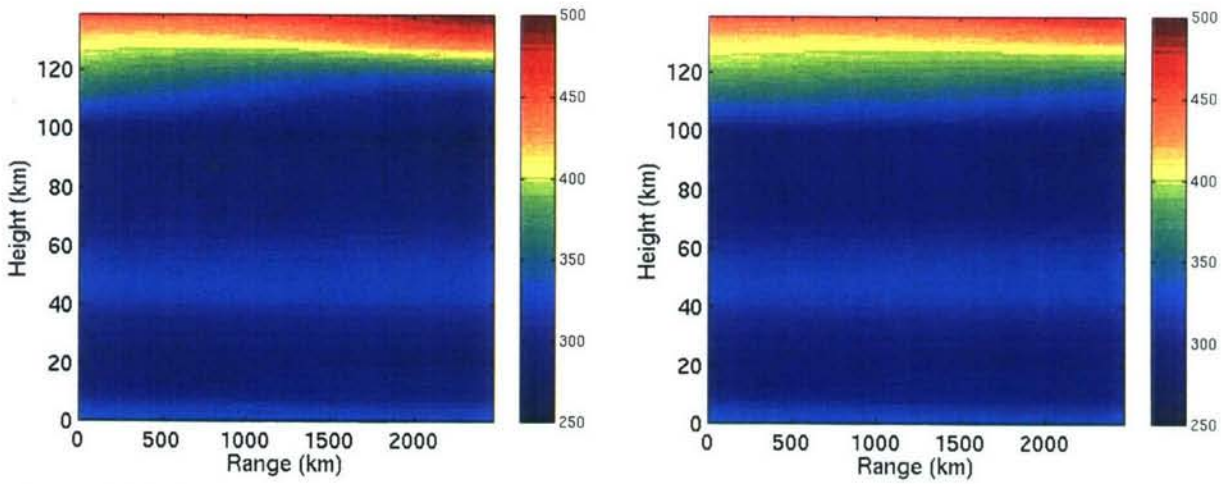

Figure 8. Effective sound speed along great circle path for evolving (left panel) and frozen (right panel) environment.

Parabolic Equation. The results predicted by the PE model in these two environmental scenarios are shown in Figure 9. Again, the panel on the left shows the evolving environment,

and the panel on the right shows the frozen environment. The effect of the environment on turning height can be seen by examination of the amplitude fields in the region of 100 to 120 km altitude. The predicted focusing effects at the ground also differ somewhat in the two scenarios.

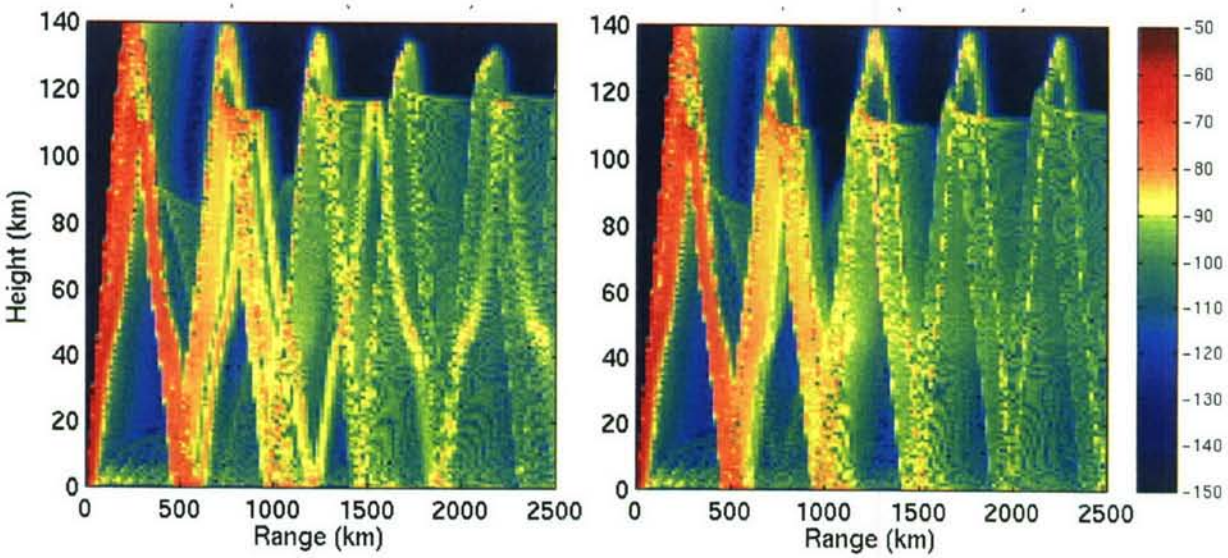

Figure 9. PE model results for evolving (left panel) and frozen (right panel) environment.

InfraMAP's capabilities can be used to examine the effects at the ground in more detail. In Figure 10, amplitude, relative to the source, is shown at the ground (0 km altitude) for both evolving and frozen environments. At certain ranges (e.g., 800 km, 1800 km), amplitude differences on the order of 20 dB can be seen.

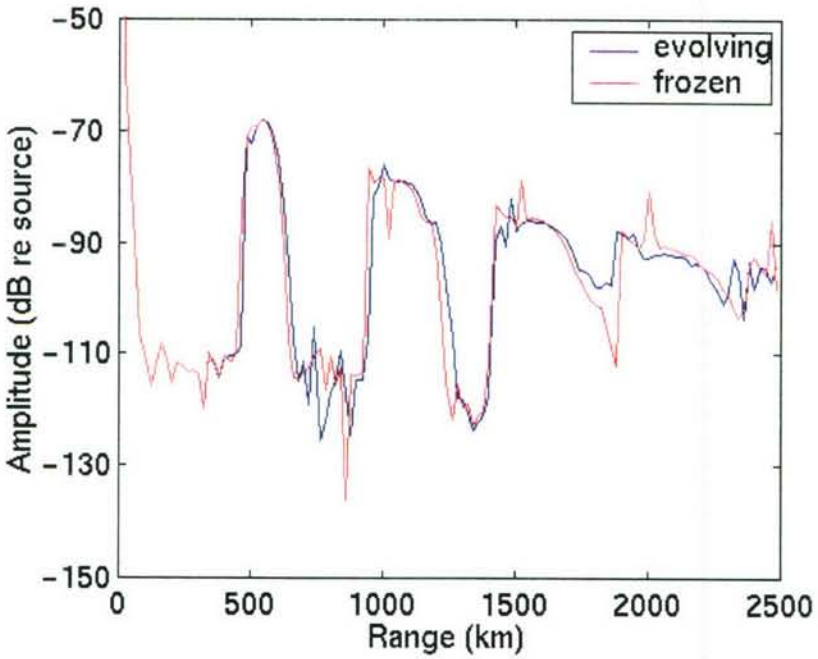

Figure 10. PE model predictions along ground for evolving and frozen environment.

Ray Tracing. When ray tracing was applied to the two scenarios, three thermospheric eigenrays were identified for each case. They are shown in Figure 11 for both the evolving and frozen environments. The travel time differences between the two sets of rays were small, on the order of 0.2%, and the azimuth deviation differences were 0.3 degree or less. However, there are significant differences in the thermospheric turning heights (up to approximately 5 km differences), in a region of the atmosphere where absorption is high and increasing rapidly with altitude.

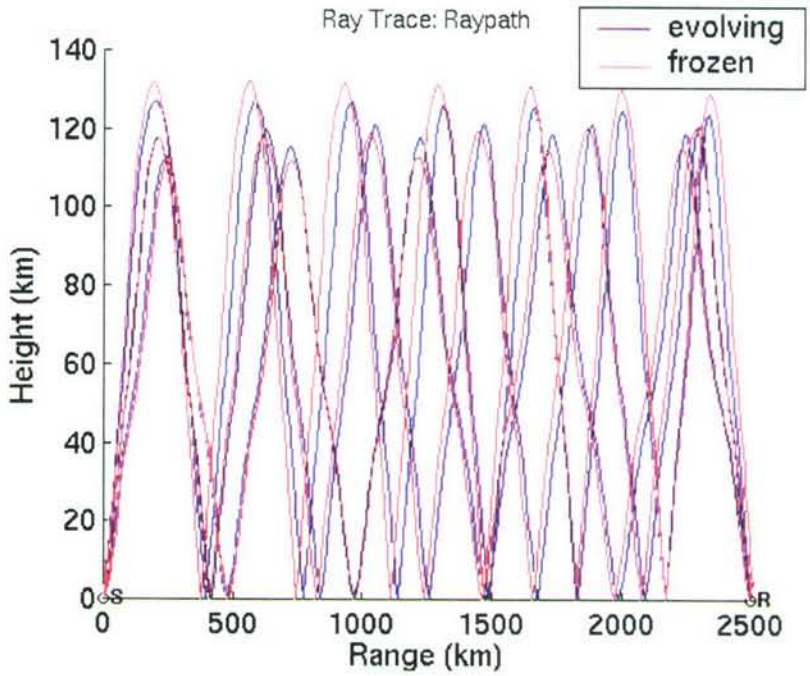

Figure 11. Ray tracing paths for evolving and frozen environment.

Acoustic absorption is calculated, using the classical absorption model, for each of the rays shown above, and presented in Figure 12. Large differences in absorption can be seen between the two cases for those paths that go high into the thermosphere (the two uppermost curves). The integrated absorption along the ray path is important because it determines the observability of the energy at a receiver location.

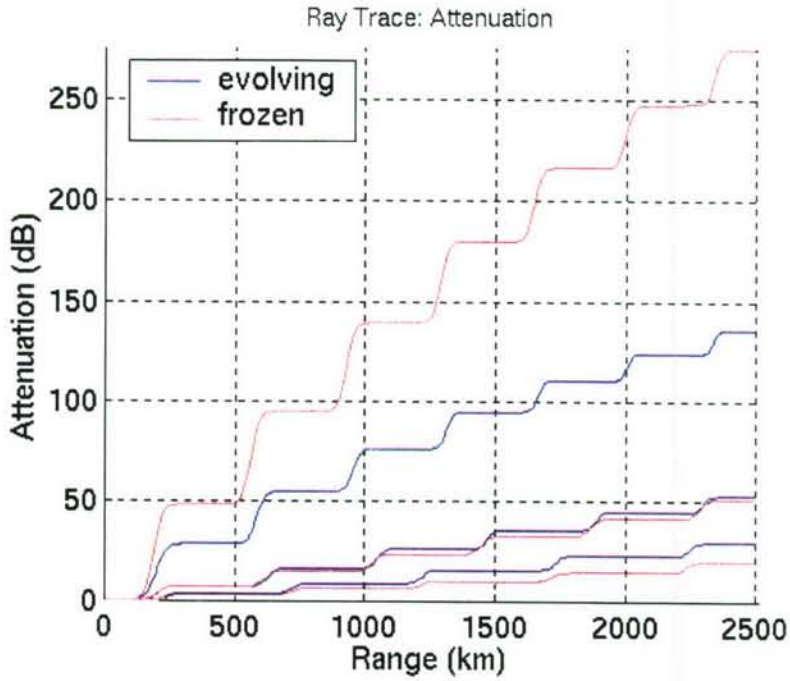

Figure 12. Attenuation along ray path for evolving and frozen environment.

4.6.2 Atmospheric Absorption.

In this study, the integrated absorption model [Sutherland and Bass, 1996] is applied to characterize the attenuation of infrasound at various frequencies. Figure 13 gives example profiles of predicted absorption coefficients at 0.2 and 0.5 Hz. Translation and diffusion losses are plotted together as classical loss, of which the diffusion loss makes up less than 1% of the sum.

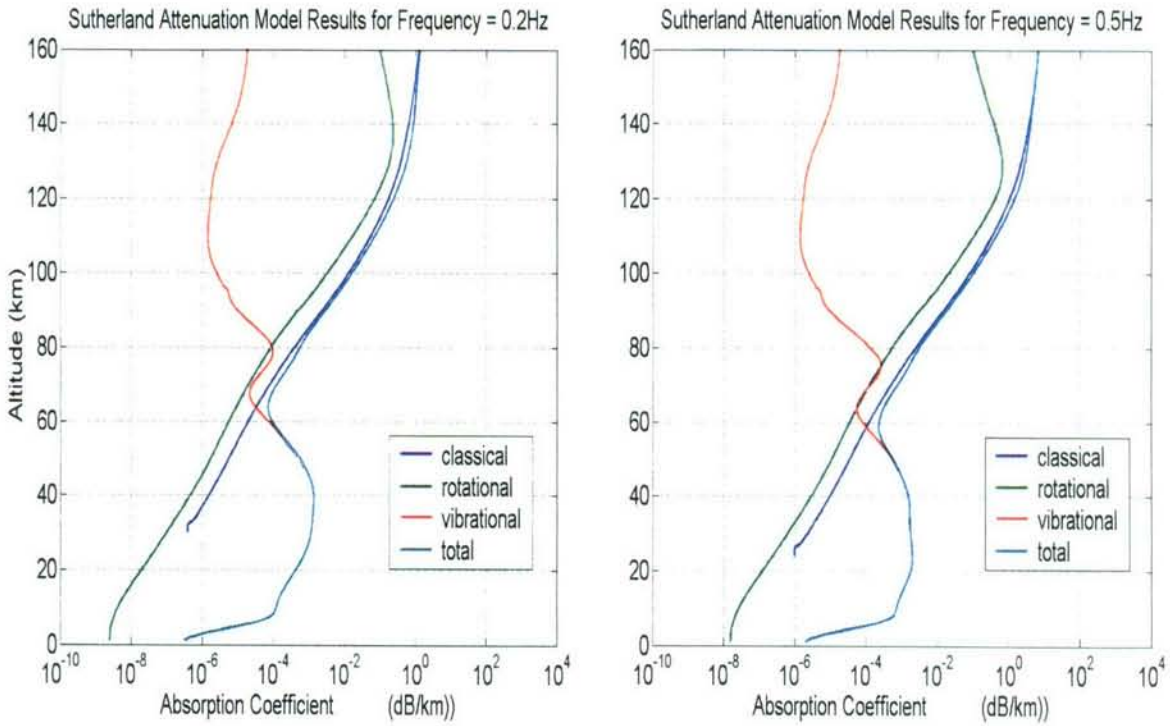

Figure 13. Absorption coefficients computed from a low frequency, high altitude model [Sutherland and Bass, 1996] at 0.2 and 0.5 Hz.

Below 60 km, vibrational loss dominates, but the total absorption is still relatively small. Propagation of a 0.5 Hz signal over a 500 km path would only experience about 0.5 dB of attenuation in this region (neglecting spreading loss). The effects are much different within the thermosphere. At 120 km, the absorption coefficient increases dramatically with frequency; at 0.2 Hz, it is 0.1 dB/km, and at 0.5 Hz it increases to 1 dB/km. Even acoustic signals that sample these regions for a small percentage of their propagation path can experience significant attenuation. As an example, a 0.5 Hz signal that spends 10% of its 500 km path at 120 km or above would have an absorption loss of at least 50 dB.

Comparisons were made of PE amplitudes with and without the atmospheric absorption effects. Results are shown in Figure 14 for a source at the ground. The amplitude predictions are made for upwind conditions, so a stratospheric return, with an upper turning height of 40-60 km, is not present. In the cases where absorption is not included, significant thermospheric energy reaches a receiver on the ground at 500 km range. With absorption included, a received signal at 500 km range would still contain a thermospheric return at 0.2 Hz, although the amplitude is reduced. However, at 0.5 Hz, the signal experiences strong absorption at altitudes between 110 and 120 km, and any thermospheric energy arriving at the receiver is heavily attenuated.

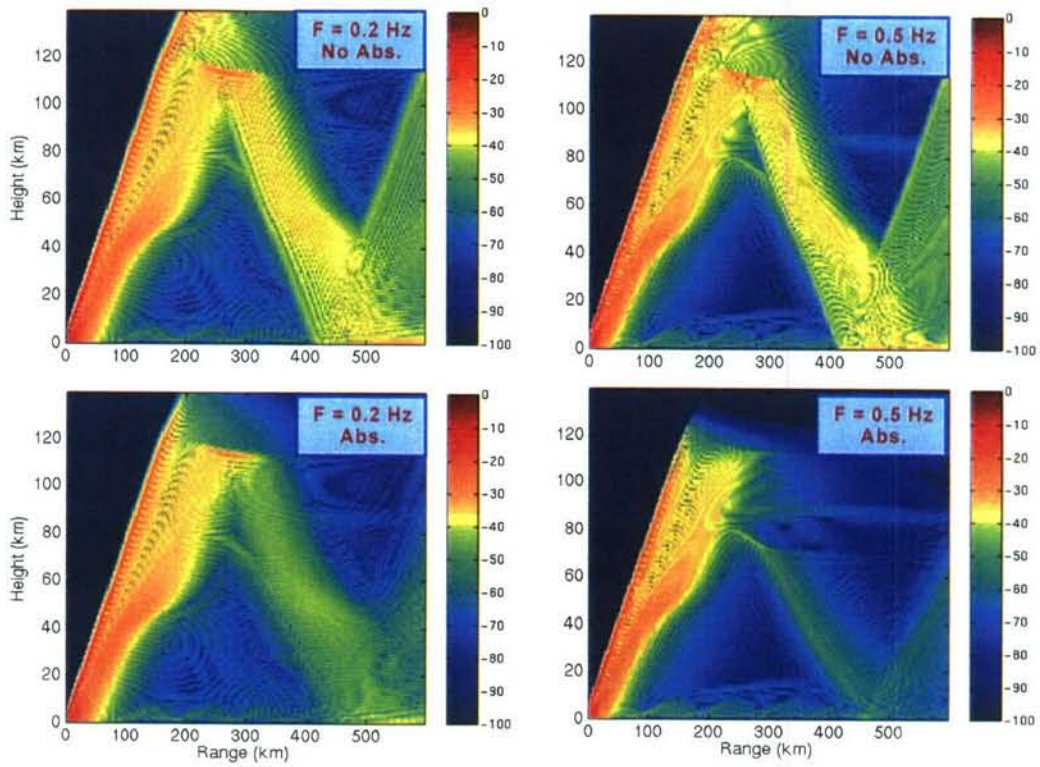

Figure 14. Comparison of PE amplitude predictions with and without absorption. Absorption effects at 0.5 Hz are apparent in the thermosphere, where energy propagating above 115 km is heavily attenuated.

Infrasonic observations are ordinarily made on the ground. Thus, it is of interest to look at the frequency dependence of PE amplitude prediction at ground level (0 km altitude). Figure 15 gives PE amplitude at the ground along a 2600 km path and a broad frequency band. The figure suggests:

- A trend of increasing frequency absorption with range
- Evolution of sharp shadow zone boundaries as frequency increases
- Shadow zone formation over limited frequency bands

It is important to note that scattering from atmospheric turbulence will tend to smear energy path boundaries. As a result, the deep attenuation predicted in the shadow zones would be reduced.

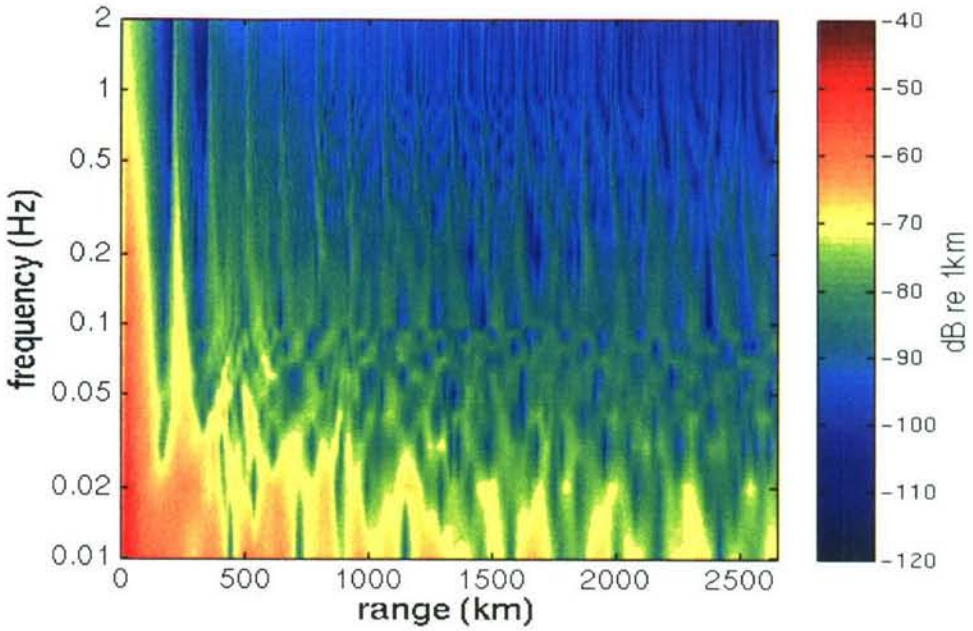

Figure 15. PE amplitude predictions along the ground over a frequency band from 0.01 to 2 Hz.

4.6.3 Global Duct Heights.

In some recent studies of infrasonic events by the research community, disagreement between predictions and observations has suggested the importance of elevated duct propagation. There have been certain observations that are characterized by signal velocities typical of stratospheric ducting that cannot be modeled with stratospheric ducts. It is hypothesized that stratospheric energy in an elevated duct is observed at the ground through diffraction and scattering. This study is focused on quantifying the distribution of elevated stratospheric ducts.

These computations are based on using HWM-93 and MSIS-90 environmental models on January 1, 2001 at 12 UT. The date corresponds to a season where strong zonal winds are present. Stratospheric ducting would be less pronounced during the transitional periods in the spring and fall when the zonal winds change direction.

The stratospheric ducts are evaluated along the maximum wind direction. Sound speed profiles are computed for the no wind (static) and counter-wind (effective) cases. The counter-wind direction is chosen to evaluate the presence of elevated stratospheric ducts for the case where no ground-based stratospheric ducts exist.

Elevated stratospheric ducts have the same upper boundary as stratospheric ducts but have a lower boundary that is above the earth's surface. The presence of elevated stratospheric ducts is found by computing the height of ducts starting at a given lower boundary. The lower boundary heights evaluated here are 5 and 10 km. The presence of stratospheric ducts was also found using a lower height of 0 km. When the duct height is above 100 km, no stratospheric duct was

found and only a thermospheric duct exists. Figure 16 shows the duct heights for the 10 km lower boundary.

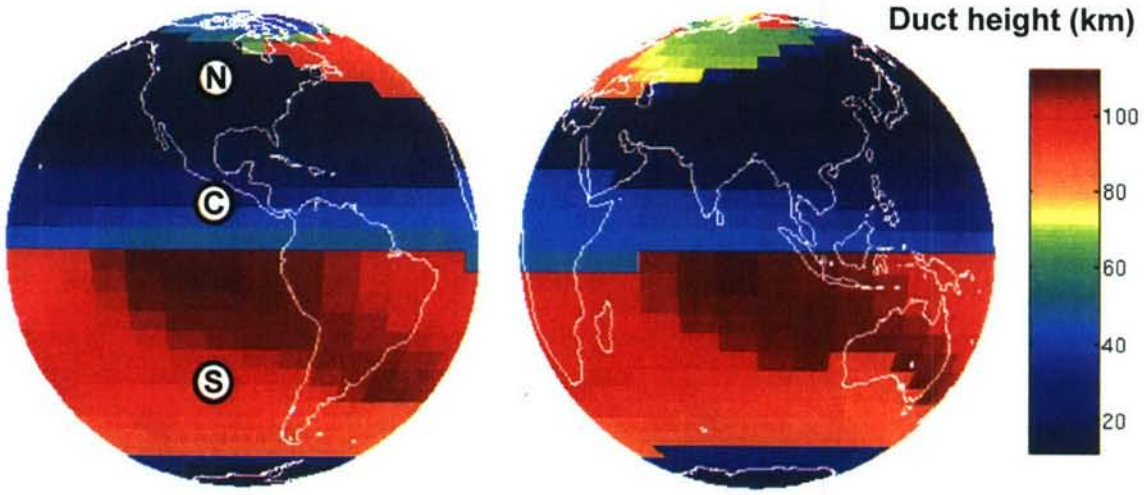

Figure 16. Duct heights for lower boundary of 10 km modeled for 1 Jan 01.

The duct height features in Figure 16 can be divided into three general regions: N, C, and S. The representative profiles for each region, using the 10 km lower boundary, are given in Figure 17 to 19. Two sound speed profiles are shown: the static case with no wind, and the counter-wind case. The green arrow shows the elevated duct that forms for the counter-wind profiles. In the southern region (S), no elevated stratospheric ducts exist as the upper height boundary is in the thermosphere. For the central region, elevated stratospheric ducts exist with upper height boundaries of approximately 50 km. In the northern region, elevated stratospheric ducts form that have upper height boundaries below 30 km.

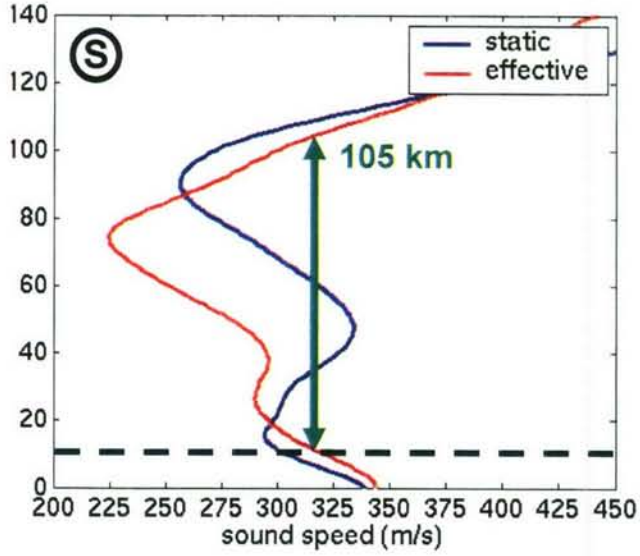

Figure 17. Static and counter-wind Sound speed profiles in region S.

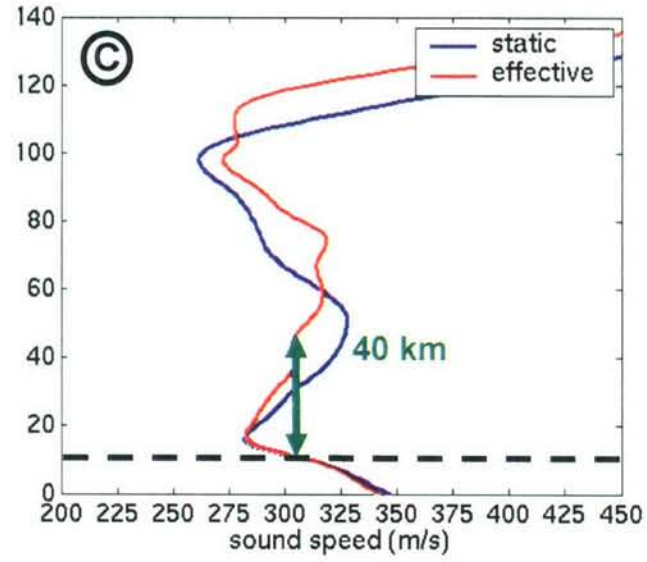

Figure 18. Static and counter-wind Sound speed profiles in region C.

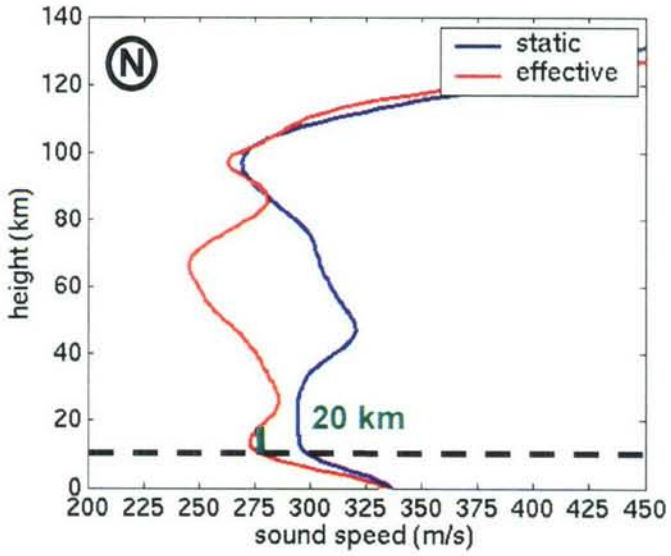

Figure 19. Static and counter-wind Sound speed profiles in region N.

Similar calculations were done at lower duct heights of 0 and 5 km. At 5 km, only a small band of elevated stratospheric ducts exist. This band is centered at approximately 20 deg North in latitude.

This study suggests that conventional propagation analysis would not predict any stratospheric propagation paths in the counter wind direction. However, by considering elevated stratospheric ducts with lower heights above the ground, stratospheric propagation can be predicted in certain regions of the globe, with the size of the region dependent on lower boundary height. To use these predictions with ground-based measurements, an assumption must be made as to how

energy leaks out of the duct and down to the ground. Diffraction and scattering are the most likely mechanisms.

4.6.4 Propagation Variability.

The goal of the propagation variability study is to quantify the bounds in travel time and azimuth that can be expected as driven by the environmental variability. To perform the study, multiple wind perturbation realizations are generated, and a Monte Carlo simulation is executed where multiple rays are traced through the sum of mean and perturbed environmental fields. The two ray parameters (travel time, azimuthal deviation) are calculated for each perturbation. The sensitivity of ray tracing calculations to variability in wind profiles is then quantified by computing the mean and variance of the predicted distributions.

Propagation variability is studied along the 1700 km path from the 23 April 2001 Pacific bolide to IS57 (Pinon Flat, California). The reference ray propagates in an elevated stratospheric duct with a lower boundary height of approximately 8 km. In the first perturbation study, the environmental variability is modeled using the range-independent gravity wave model. Thus, a signal perturbation profile is used at all ranges for each realization. Twenty perturbed rays are computed and shown in Figure 20 along with the reference ray. The perturbed rays deviate from the reference ray but still follow the same general ducted path.

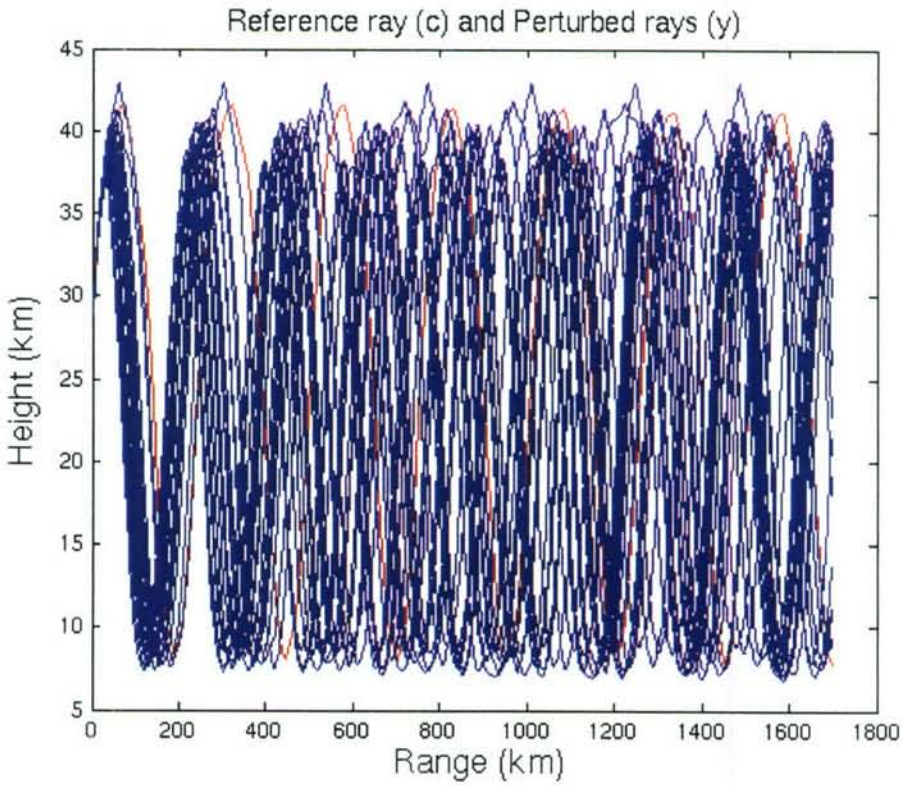

Figure 20. Reference and perturbed rays using the range-independent gravity wave model.

The travel-time distribution for the perturbed rays is given in Figure 21. The small sample size tends to distort the distribution but it roughly resembles a normal distribution. The mean travel time is 5813 s and the standard deviation is 44 s. The minimum and maximum are approximately 100 s plus and minus the mean value.

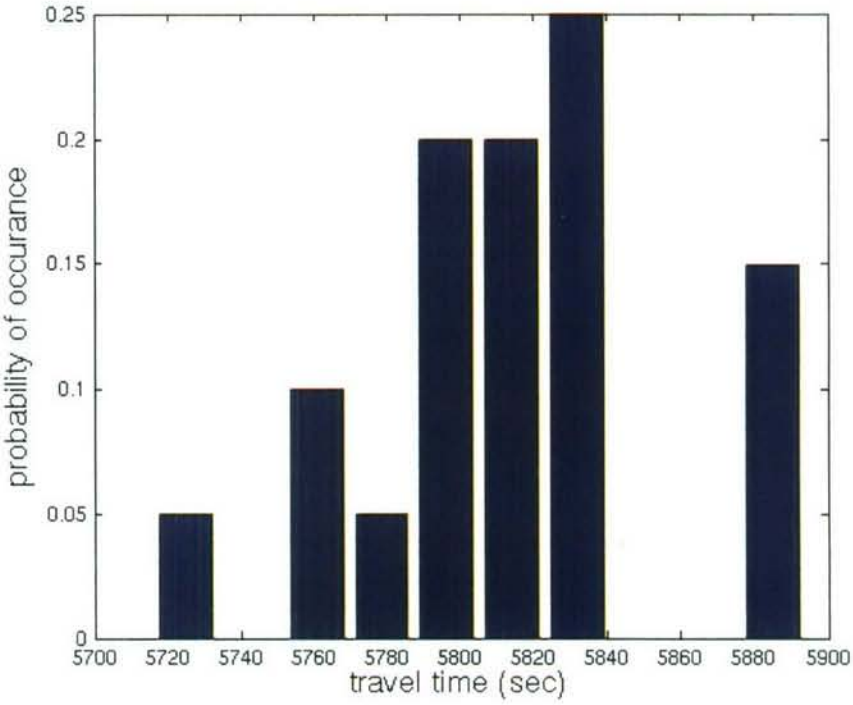

Figure 21. Travel-time distribution using the range-independent gravity wave model.

The same variability is also studied using a range-dependent gravity wave model. Here the wind perturbation realizations are not profiles but range-height fields, as shown in Figure 5. Two perturbed rays along with the reference ray are shown in Figure 22. These perturbed rays deviate fundamentally from the reference ray in that they are trapped in secondary transient ducts. These transient ducts result from the wind perturbation field and exist over the horizontal length scale of the gravity wave model (selected to be 500 km in this case). Perturbed rays that are trapped in transient ducts make up about 15 percent of the total number of realizations.

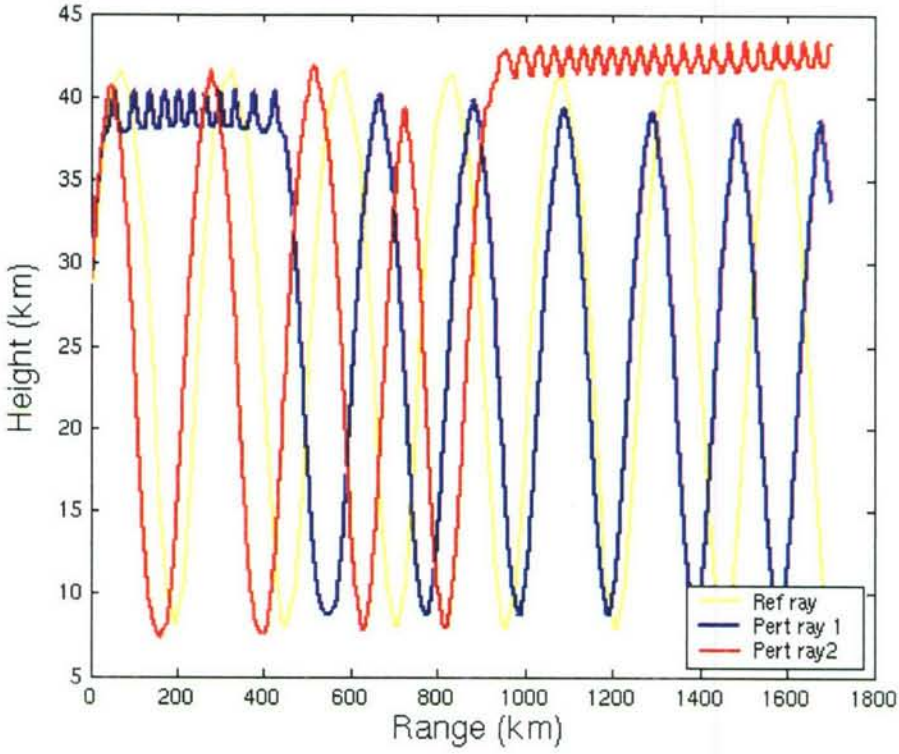

Figure 22. Reference and two perturbed rays using the range-dependent gravity wave model.

The associated travel time distribution is shown in Figure 23. The mean is 5788 s and the standard deviation doubles to 85 s. Of greatest interest is that the distribution now has outliers outside of the main distributions, corresponding to the perturbed rays trapped in the transient ducts. The resulting travel times are approximately 300 s earlier than the mean, and the corresponding signal velocities are in the range of .310 km/s. These velocities are faster than the mean value of 0.294 km/s, the latter more typical of stratospheric rays.

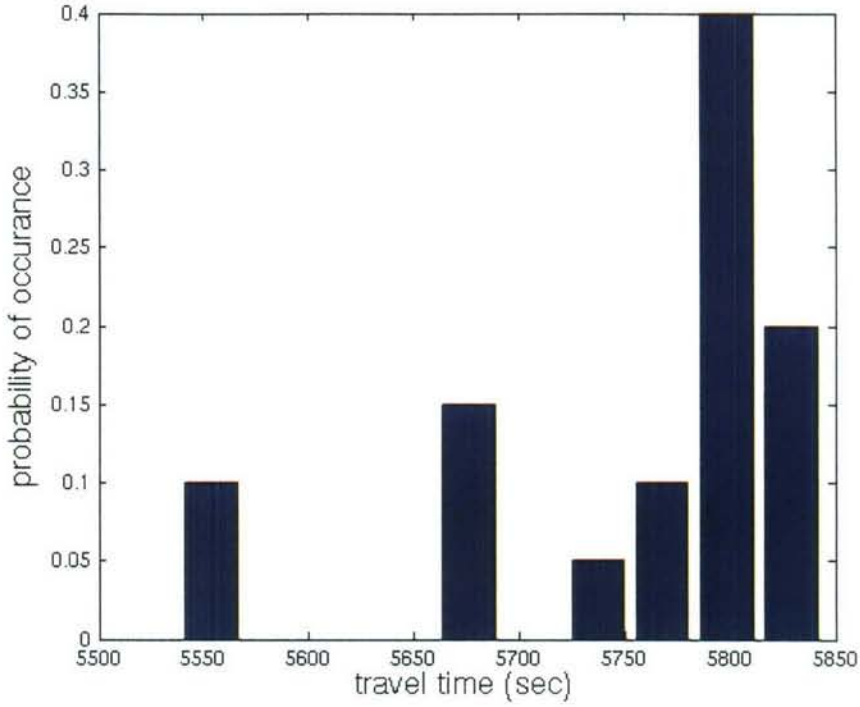

Figure 23. Travel-time distribution using the range-dependent gravity wave model.

This study has shown that new propagation features can be seen with the introduction of range-dependence in the environmental variability models. The range-dependent gravity wave model more realistically models the horizontal scales associated with gravity wave observations. The perturbed rays suggest that energy can get trapped within shallow transient ducts that form between gravity wave layers. One modeling effect of this propagation mode is a reduction in the overall travel time and increase in signal velocity.

4.7 Validation Studies.

Several validation studies have been performed using infrasonic sources of opportunity. Launches of the space shuttle provide a strong moving source that travels from the ground into the thermosphere. Bolides are another excellent infrasonic source. They move at hypersonic speeds and fragment (explode) at some point along their trajectory.

4.7.1 Space Shuttle.

Rocket launches may serve as useful ground truth data for infrasound [McLaughlin *et al.*, 2000] and also represent an excellent source of opportunity for model validation. Space shuttle launches have been observed at Los Alamos (DLIAR) and at Lac du Bonnet (IS10), among other locations.

Rocket and missile launches from the Eastern US were observed extensively in the 1960's and 1970's at Palisades, NY and elsewhere, and a series of reports describing them (for example, [Balachandran and Donn, 1971]) were issued by scientists at Lamont-Doherty Geological Observatory and the US Army Electronics Command. A number of important findings resulted from this early work, including:

- Characterization of seasonal dependency;
- Quantification of wind effects on azimuth;
- Identification of two distinct source regions, one near the launch site and one near the re-entry location of the first stage;
- Association of source location with high-velocity portions of the trajectory in high-density regions of the atmosphere.

NASA's space shuttle is launched from Cape Kennedy, Florida a few times per year. During the spring and summer of 1999, the launches of two shuttle missions were observed at infrasound stations DLIAR and/or IS10.

BBN used a commercially available launch simulator software package to determine the trajectories for these specific missions, using actual launch parameters. The software was also used to estimate trajectories for the solid rocket boosters, which are released from the orbiter approximately 2 minutes into the ascent. Modeled trajectories for the two observed shuttle missions, STS-96 (27 May 99) and STS-93 (23 July 99) are shown in Figure 24. Launch ascent trajectories for the STS-96 orbiter and solid rocket boosters (SRBs) are shown in Figure 25. (The modeled STS-93 ascent trajectories are very similar to those for STS-96.)

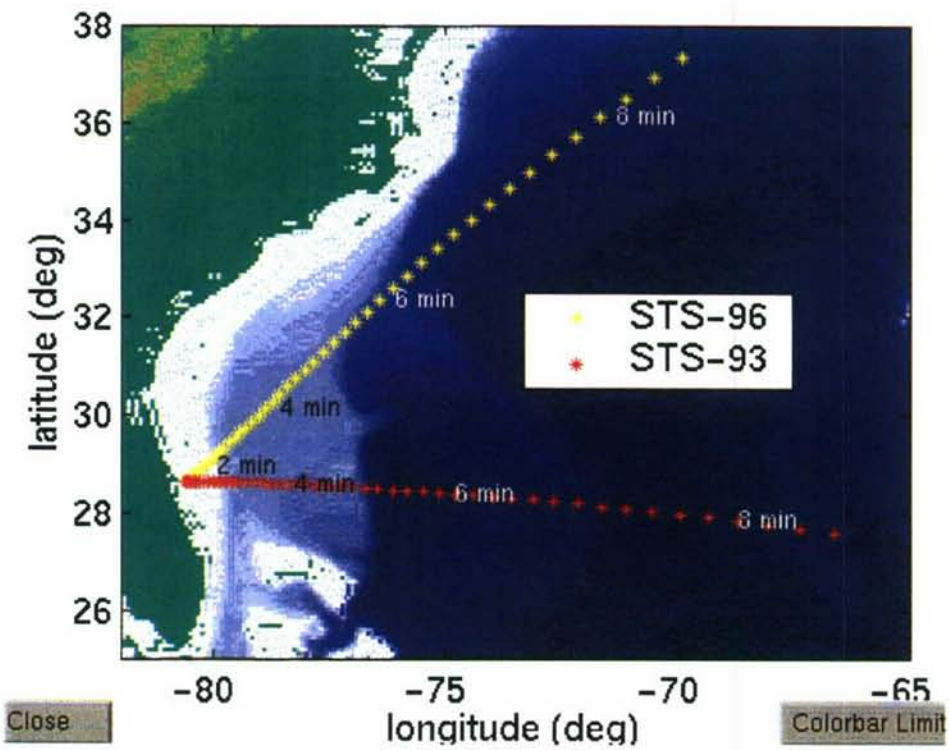

Figure 24. Space shuttle trajectories for two missions.

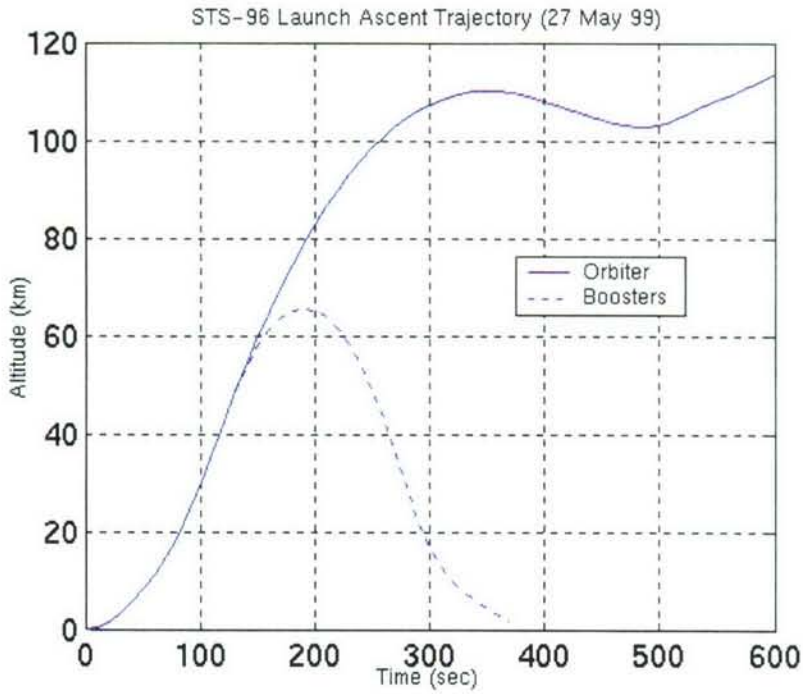

Figure 25. Space shuttle orbiter and booster trajectories.

InfraMAP was used to determine eigenrays to DLIAR from points along the STS-96 trajectory, with HWM-93 and MSISE-90 used for environmental characterization. The continuously moving source was modeled as a series of discrete sources separated in space and time. A source was modeled every 10 seconds from the launch time out to 5 minutes after launch for the orbiter and from 200 seconds out to 6 minutes after launch for the solid rocket boosters (SRB). For each eigenray, an arrival azimuth and an arrival time (referenced to the launch time) were determined. Results are shown in Figure 26. Stratospheric rays and thermospheric rays are depicted separately for both the orbiter and the SRB. Also shown in the figure (as red asterisks) are results from the observation at DLIAR, determined by analysis using InfraTool and MatSeis software, and provided by Dr. Rod Whitaker of DoE/LANL and Dr. David Brown of CMR.

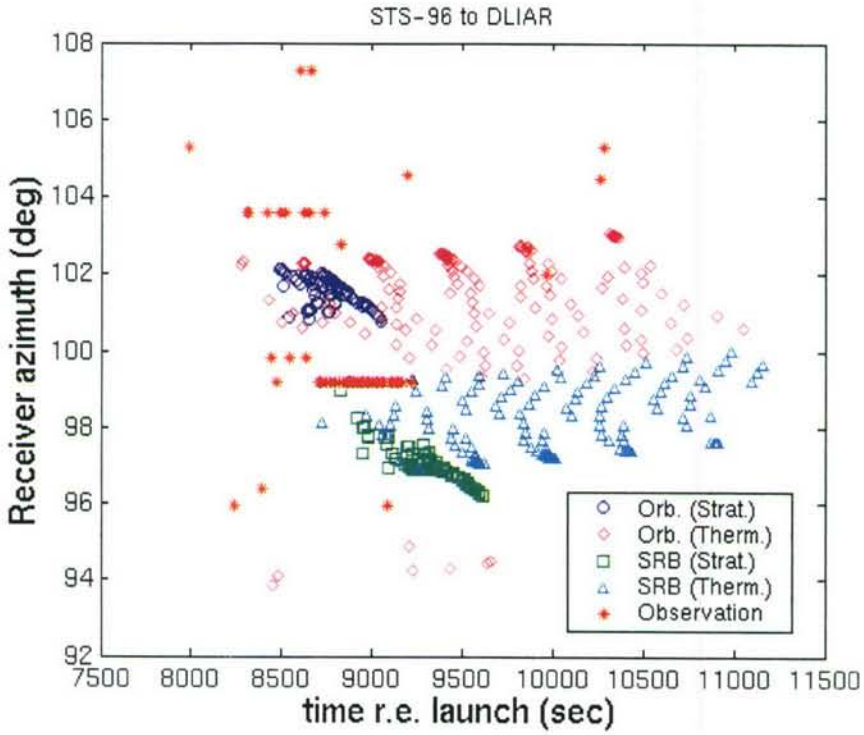

Figure 26. Predicted and observed infrasound arrivals from STS-96 to DLIAR.

The two primary observed arrivals (at approximately 103.5 and 99 degrees) are reasonably well modeled by the stratospheric rays from the orbiter (blue circles) and boosters (green squares), respectively. However, a bias in azimuth of approximately 2 degrees can be seen for both primary arrivals. Further modeling of the launch event using an updated atmospheric characterization, in order to see if travel time and azimuth predictions could be improved, would be of great interest in this case.

Infrasound from space shuttle launches has also been observed at an infrasound array operated by the Army Research Lab (ARL) at Blossom Point, Maryland. [Tenney and Noble, 2000] InfraMAP was used to model propagation from the launch of the STS-88 mission (04 Dec 98), again using HWM-93 and MSISE-90. The STS-88 trajectory was similar to that of STS-96 shown above. Similar time steps and durations were used for the source model. A spectrogram of the observation at Blossom point (data provided by Mr. Steve Tenney and Dr. John Noble of ARL) is shown in Figure 27. An azimuth vs. time diagram is shown in Figure 28. The white "dotted line" boxes have been added to Figure 28 to denote the primary arrivals.

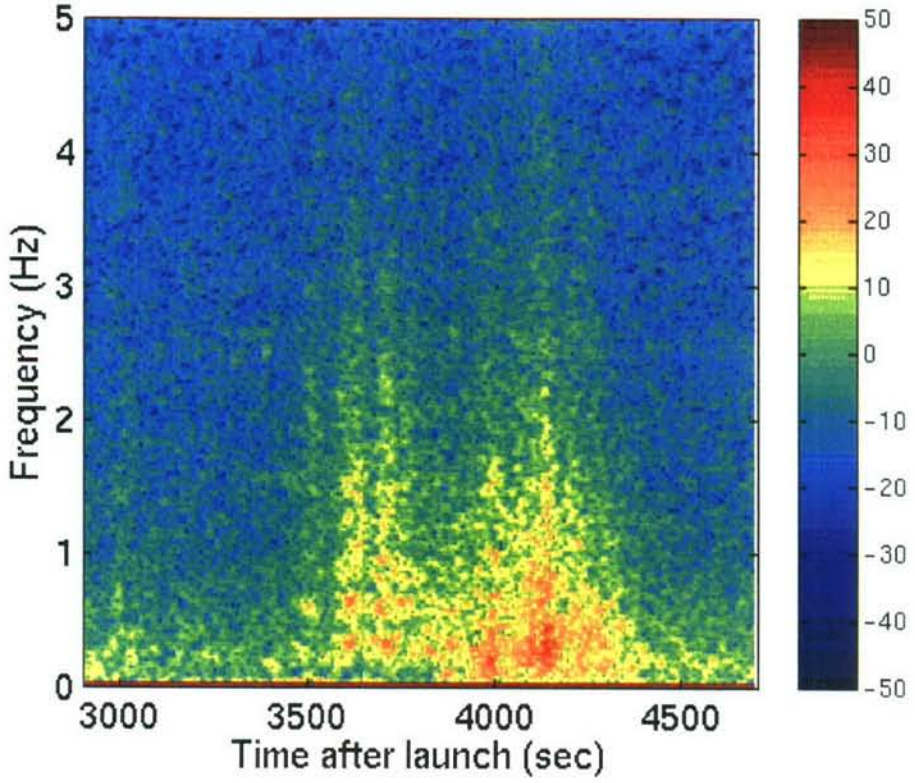

Figure 27. Observed infrasound signal from STS-88 to Blossom Point.

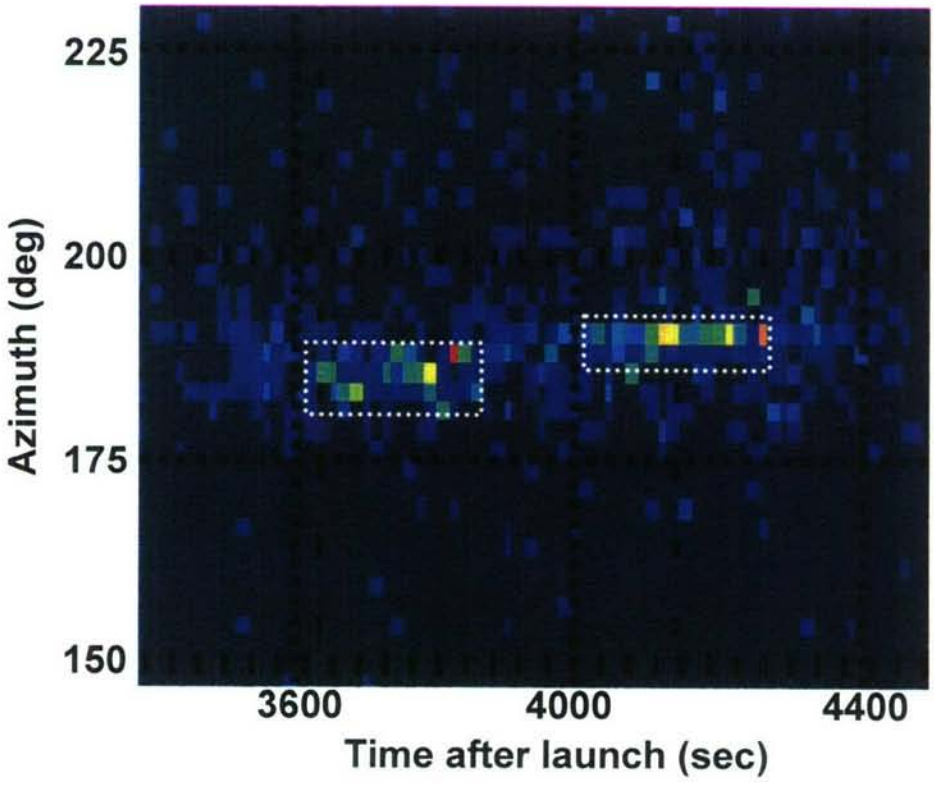

Figure 28. Observed infrasound arrivals from STS-88 to Blossom Point.

Eigenray results from InfraMAP are shown in Figure 29. Overlaid on the predictions are red "dotted line" boxes that correspond to the arrivals as depicted in Figure 28. In this case, the increasing azimuth trend is well modeled by both the stratospheric and thermospheric rays. There is a bias in travel time of approximately 300 seconds between the observed arrivals and the modeled stratospheric rays. The modeled stratospheric rays from the boosters (green squares) arrive before those from the orbiter (blue circles) because the source is moving supersonically toward the array.

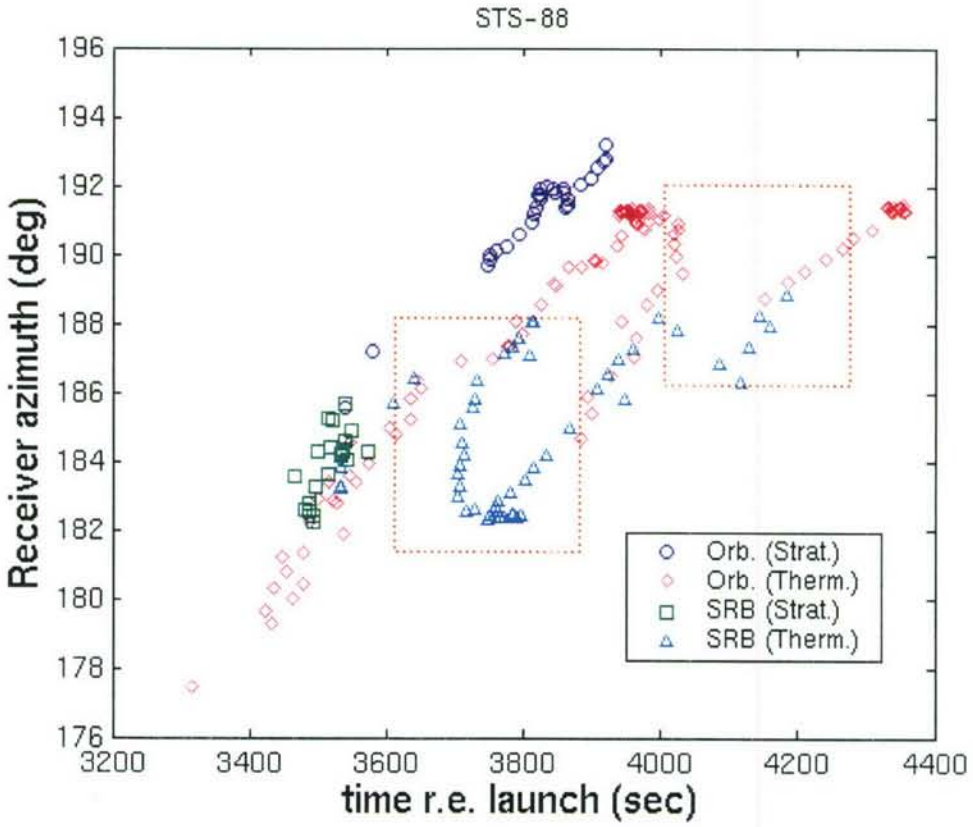

Figure 29. Predicted and observed infrasound arrivals from STS-88 to Blossom Point (red boxes depict main observed arrivals, as shown in Figure 27).

Further research into several technical issues has been ongoing under a separate contract effort, including: modeling improvements achievable with near-real-time updates as compared to HWM-93 and MSISE-90; further understanding of the infrasound source mechanism in order to identify the regions of the trajectory (altitude, velocity, etc.) that contribute most strongly to observed signals; and quantifying attenuation along the ray paths to support identification of observed phases.

4.7.2 El Paso Bolide

On 9 Oct 1997, a large bolide traveled above Texas near El Paso. The height of the bolide, as determined from satellite observations, was 29 km. This bolide was detected at both the Los Alamos DLIAR array (range 445 km) and the Southern Methodist University TXIAR array (range 359 km). The received data at TXIAR has been studied to evaluate the ability to verify or refine the source height estimate.

To model the bolide signal, eigenrays were computed over a range of source height from 0 to 50 km. Figure 30 shows the eigenray solutions at 30 km source height. Over the range of heights, there are 1-3 stratospheric eigenrays and 2-3 thermospheric eigenrays.

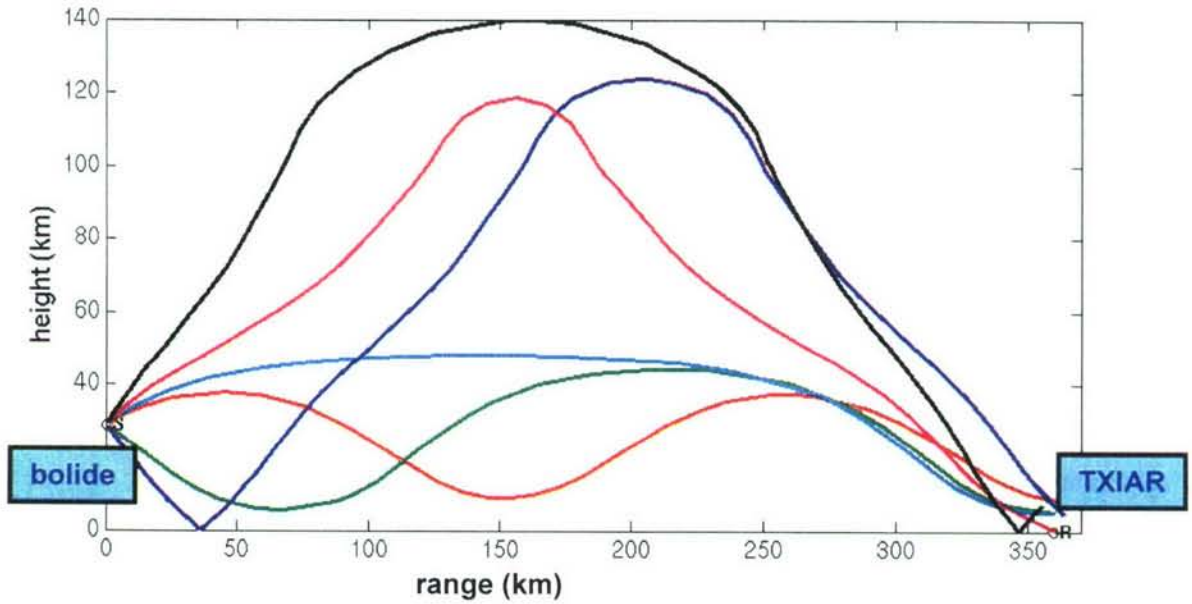

Figure 30. Eigenray solution between El Paso bolide at source height of 30 km and receiver at TXIAR.

Synthetic waveforms were next computed for each source height and mapped into an image as a function of arrival time and source height (bottom of Figure 31). A Gaussian waveform of standard deviation 10 sec was used as the source function. For sources near the ground, single eigenrays can be observed, which then split into multiple eigenrays at the height increases. The split rays for a given v-shaped branch correspond to two similar paths, one propagating up at the source, the other propagating down, reflecting off the ground, and then propagating up. The eigenray image can be compared to the measured waveform (top of Figure 31), and a source height estimate can be made by correlating the measured arrival times with the predicted amplitudes. The three measured arrivals match the predictions at source heights of 33, 26, and 23 km, respectively. Although there is a spread in these heights, they are in general agreement with the satellite-determined source height of 29 km.

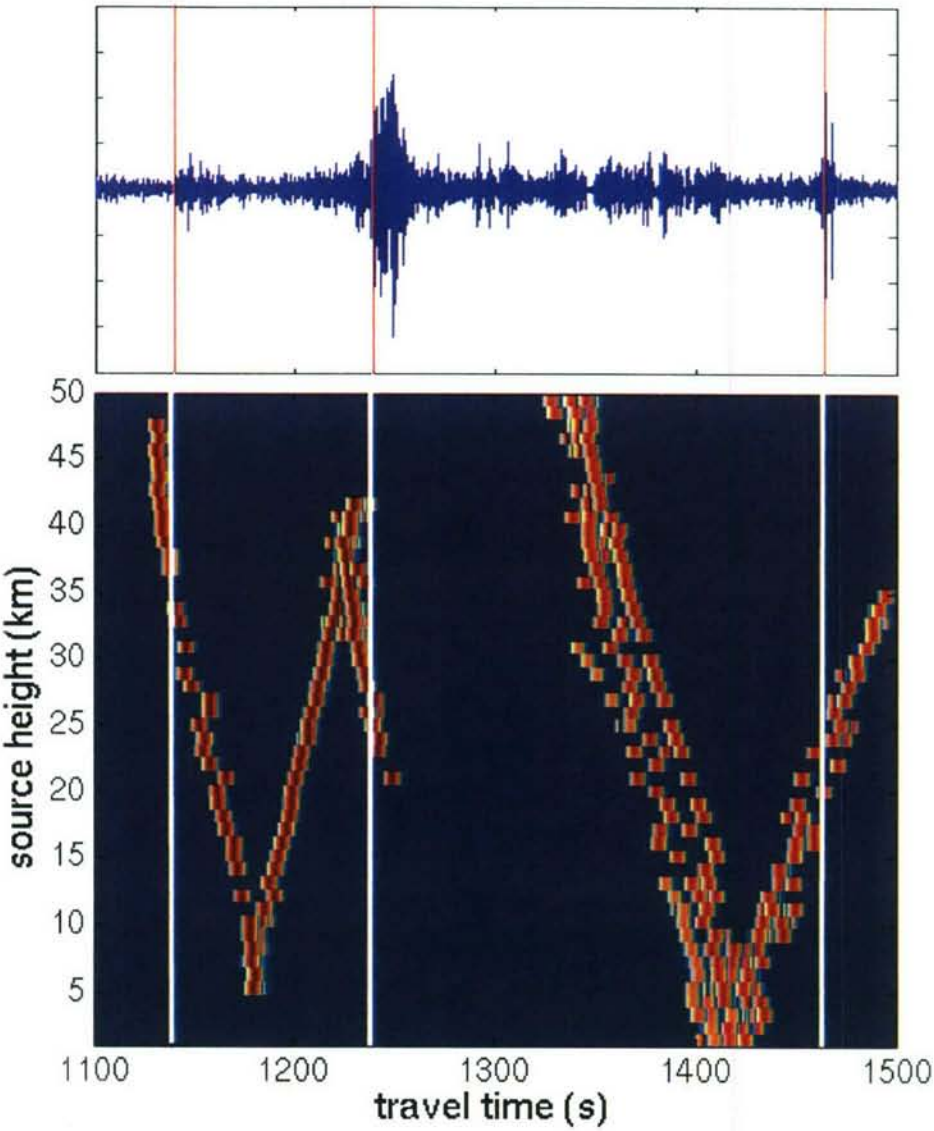

Figure 31. Comparison of measured arrival times (above) with synthetic waveform prediction from eigenrays solved over 0 to 50 km (below).

4.7.3 Tagish Lake Bolide

On 18 January 2000, sensors aboard DOD satellites detected the impact of a meteoroid at 16:43:43 UT near Whitehorse in the Yukon Territory, Canada. The object detonated at an altitude of 25 km at 60.25 degrees North latitude, 134.65 degrees West longitude [Brown *et al.*, 2002]

An infrasonic signal was detected at the IMS station in Lac du Bonnet, Canada, a range of 2641 km from the bolide. A received waveform is shown in Figure 32. This waveform is filtered over

the frequency band of 1.0 - 1.5 Hz. The main arrival appears at an arrival time of approximately 8200 sec. There may also exist a secondary arrival at 11,300 sec.

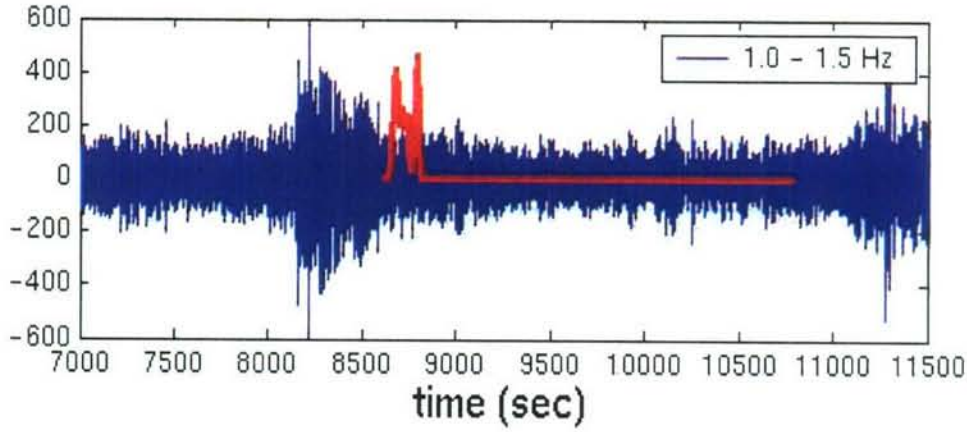

Figure 32. Filtered waveform measured at Lau de Bonnet IMS station (blue), and synthetic waveform generated from eigenrays (red). Amplitude units are arbitrary.

Measurements across the 3 elements of the array were beamformed using an F-K processing algorithm. The results were inconsistent across the observed waveform, possibly due to low signal-to-noise ratios or loss in coherence of the signals across the array, resulting from turbulence. The strongest coherent cluster in the F-K slowness plane was found using a time window from 8400 - 8500 sec and a frequency band of 0.2 - 1.0 Hz. The back azimuth for this cluster was 306.5 deg.

Eigenrays were computed for this path and are shown in Figure 33. Both stratospheric and thermospheric rays are present. The stratospheric rays have back azimuths at approximately 310 deg, and the thermospheric at approximately 311 deg. These predictions differ by several degrees from the measured value of 306.5 deg.

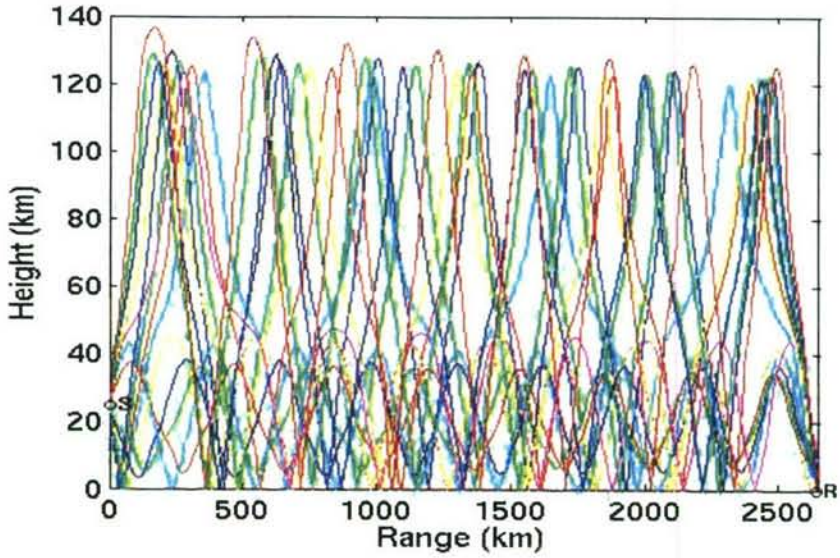

Figure 33. Eigenrays from Tagish Lake bolide to Lac du Bonnet IMS station.

Synthetic waveforms were generated from the eigenrays for comparison with the measurements. The source function was a Gaussian waveform with a standard deviation of 10 sec. The predictions are overlaid on the waveforms in Figure 32. A bias of approximately 500 sec is apparent in the arrival times. This difference may be due to discrepancy between the predictions of temperature and wind from the HWM-93 and MSISE-90 models and the actual environmental conditions during the propagation. It may also result from inadequate modeling of the source function.

4.7.4 Pacific Bolide

In this study, the 23 April 2001 Pacific bolide is used to evaluate the network localization capabilities integrated into InfraMAP. This bolide is an excellent source of opportunity because ground truth in latitude, longitude, and height is available and infrasound from the bolide was observed at a large number of stations.

Figure 34 shows the location of the bolide and the six infrasound stations with observations used to localize it. Note that the IS26 station in Freyung, Germany is not shown in the figure, the great circle path length for this case being over 9000 km.

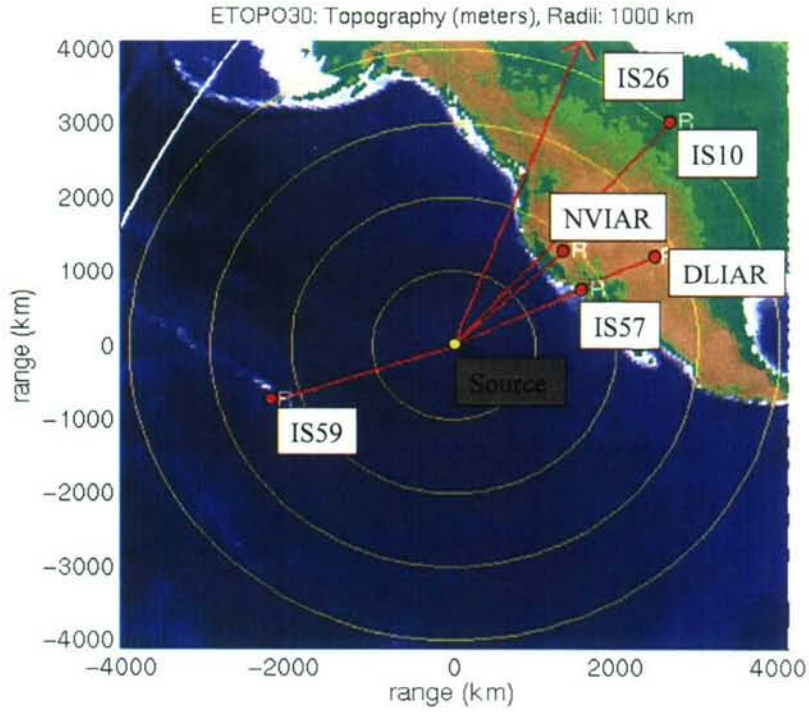

Figure 34. Location of the 23 April 2003 Pacific bolide along with the six stations used to localize it.

The localization is based on measured arrival times, back azimuths, and associated measurement errors recorded at the stations. A baseline localization has been computed using these data and signal velocity tables [Brown *et al.*, 2001]. To fully utilize the integrated localization capabilities in InfraMAP, additional estimates of azimuthal deviation, and propagation uncertainty due to the environment are needed. These values are computed by using an event-specific propagation modeling to classify the ray phase (propagation mode) from the bolide to each station [Norris, 2003; Norris and Gibson, 2002a]. This approach also estimates signal velocity, eliminating the need for look-up tables.

The model-based approach starts by using the baseline localization as an initial source reference point for the modeling. A fan of rays is reverse propagated from each station back toward the source. These rays are then identified and grouped into phases (either stratospheric or thermospheric). Two ray parameters are computed for each phase: signal velocity and azimuthal deviation. Likewise, these parameters are computed using the reference source position and station measurements. The two versions of the parameters are compared, and the modeled phase that provides the best match is identified.

Total azimuth and travel-time uncertainty is computed as the sum of the measurement error plus a contribution based on the uncertainty in characterizing the propagation. The latter is found by propagating rays through perturbed realizations of the environment and building up a set of azimuth and travel-time predictions for which variances can be extracted. The environmental

realizations are found using the spectral gravity wave model that models the relevant spatial variability in winds.

The model-based localization is calculated using the same MLE algorithm as used in the baseline localization but with several key enhancements:

- the mean signal velocity for the modeled phase is used;
- the azimuthal deviations for the modeled phase is used and added to the measured back azimuths to correct for horizontal propagation effects;
- new estimates of travel time and azimuthal uncertainty are used that include propagation variability and measurement error.

The resulting localizations are given in Figure 35. A localization based solely on azimuthal data is shown in yellow. The lack of complete azimuthal coverage of the stations is evident in the elongation of the error ellipse along an azimuth aligned with most of the stations. A localization using only arrival time data is shown in green. Here the geographic distributions of the stations results in an error ellipse aligned perpendicular to the general station direction. Finally, the localization based on all data is shown in cyan. The resulting error ellipse is significantly reduced and has an AOU of 8700 square km, and the localization has a small 29 km miss distance when compared to ground truth.

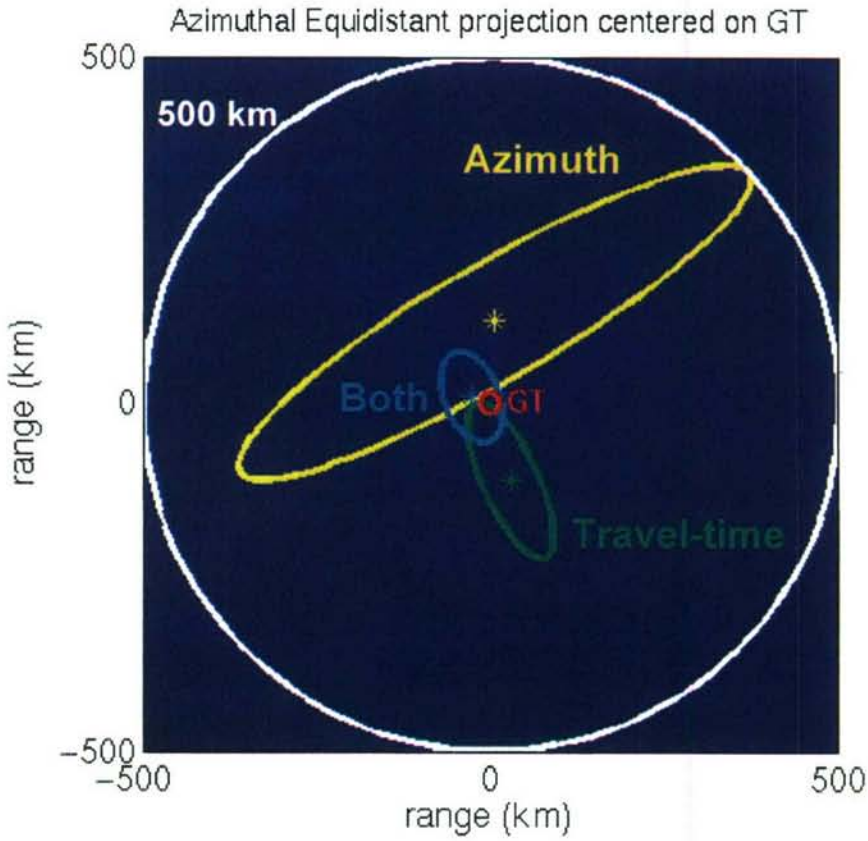

Figure 35. Model-base localization using only azimuth data (yellow), travel-time data (green) and all data (cyan).

The model-based approach to localizing the Pacific bolide showed an approximately 90% improvement in both localization accuracy and reduced AOU when compared with the baseline localization. The Pacific bolide example illustrates the excellent performance of the model-based localization approach.

Section 5
Conclusions and Recommendations

Under this effort, several enhancements have been made to the InfraMAP tool kit that facilitate advanced modeling and analysis of long-range infrasonic propagation. These enhancements have been applied to several sensitivity and special event studies. The major highlights of the project are detailed below.

Absorption

An absorption model developed for low frequencies and high altitudes has been integrated into the package. Absorption is particularly significant within the thermosphere. PE modeling for upwind propagation over a 500 km path indicates that thermospheric energy becomes heavily attenuated as the frequency increases from 0.2 to 0.5 Hz.

Synthetic Waveforms

A synthetic waveform capability has been added to the ray model. The source waveform can be specified as a blast waveform, Gaussian waveform, or user-defined waveform. The source waveform is convolved with ray arrival times and weighted by ray attenuation factors to synthesize a received waveform.

Environmental Variability

Gravity waves are believed to be the dominant source of environmental variability that affects infrasonic propagation. A gravity wave spectral model has been integrated into InfraMAP based upon scale-independent diffusive filtering arguments. From the model, realizations of wind perturbation profiles are generated. The profiles are based upon five separate spectra in the vertical direction and one dominant Gaussian length scale in the horizontal direction.

Network performance

A network performance model has been integrated that can provide source localization based on measured back azimuth and arrival times across a local network of infrasonic stations. The model allows for integration of results from propagation modeling, including the effects of environmental variability.

Propagation variability

Propagation variability has been studied by propagating rays through perturbed profiles, and Monte Carlo statistics found for travel time and azimuthal deviation. These characterizations have been used to evaluate network performance over a group of sensors by computing AOU confidence bounds for the source localizations.

Recent variability modeling studies indicate the presence of transient ducts that can significantly perturb travel times and signal velocities. These ducts form around localized minima in the sound speed, and their extent is determined by the horizontal correlation length of the gravity waves.

El Paso Bolide

Large bolides provide a strong source for infrasound and, in conjunction with ground truth data from satellites, have been used to evaluate the performance of the models. Source height estimates of the El Paso bolide have been made over a 400 km path. Synthetic waveforms were computed from eigenray solutions over a range of hypothesized heights and compared with the detected arrivals in the measured waveform. The predicted heights all fell within 6 km of the ground truth height, suggesting that multipath arrivals can be used to estimate source height.

Pacific bolide

Data from the Pacific bolide detected at six stations was used to perform multi-station source localization. The localization included detailed propagation path modeling and evaluation of environmental variability effects. The resulting location provided a more accurate localization and 90 % smaller error ellipse when compared to a table-based localization approach. The most important factor in localization accuracy was found to be correct classification of the ray paths.

Elevated duct

Elevated stratospheric ducts above 10 km can form over large regions of the globe. These ducts can be excited by either elevated sources or ground source energy that leaks into duct. It is hypothesized that this energy can reach ground-based stations through scattering and diffraction.

Recommendations and research topics that would support improved modeling of infrasonic events are listed below.

- The Tagish Lake bolide predictions suggest the possibility that a bias exists in the environmental models for the day and time of this event. Further improvements to the environmental models in InfraMAP should be investigated. In addition, data assimilation of empirical models with *in situ* measurements should be pursued to increase the accuracy of the propagation predictions.

- The gravity wave model can be improved by including the geospatial dependence on the amplitude scale factor. Other issues that should be examined include: mean plus perturbation superposition, mean flow bias, max flow limits, anisotropy, and zonal vs. meridional flow dependence.

- The largest errors contributing to source localization uncertainty are generally in the back azimuth estimates. Improvements in either the array geometries or beam-forming algorithms would be desirable to help reduce this error term.

- Network performance studies need to be done over a variety of scenarios and environmental conditions. In areas of high station density, the localization AOU can be small, while in areas of sparse coverage they can become quite large. Defining these regions of best and worst localization accuracy is critical to evaluating the overall performance of an infrasound network.

- General analysis of future bolides needs to continue. This will be facilitated by collaboration with the satellite community and with the international community. Bolide source modeling needs to improve, particularly in the areas of source mechanics, transition region where the blast wave can be modeled as a linear propagating wave, and light curve to acoustic source waveform correlation.

- Ray classification techniques need to be evaluated and improved. Use of additional discriminators, such as phase arrival envelope and amplitude, may provide new classification approaches.

- Non-linear propagation effects, such as waveform steepening and multi-shock merging, need to be researched for infrasonic sources. These effects may be particularly significant for hypersonic sources, such as bolides and reentry vehicles.

- The frequency dependence on wave propagation and travel-time predictions needs further research. In particular, the limits into the applicability of ray theory to infrasonic propagation have not been adequately defined. More research needs to be done in developing and evaluating broadband propagation models, such as the Time-Domain Parabolic Equation (TDPE) model.

Section 6
References

Balachandran, N. and W. Donn, 1971: Characteristics of infrasonic signals from rockets, *Geophys. J. R. Astr. Soc.*, **26**, 135-148. (UNCLASSIFIED)

Brown, P., D. O. ReVelle, E. Tagliaferri, and A. Hildebrand, 2002: An entry model for the Tagish Lake fireball using satellite, seismic and infrasound records, *Meteoritics and Planetary Science*, **37**, No. 5, 661-677. (UNCLASSIFIED)

Brown, D., A. Gault, R. Geary, P. Caron, and R. Burlacu, 2001: The Pacific Infrasound event of April 23, 2001, *Proceedings of the 23rd Seismic Research Review*, Jackson Hole, Wy. (UNCLASSIFIED)

Dighe, K. A., R. W. Whitaker, and W. T. Armstrong, 1998: Modeling study of infrasonic detection of a 1 kT atmospheric blast, *Proceedings of the 20th Annual Seismic Research Symposium*, Santa Fe, New Mex. (UNCLASSIFIED)

Farrell, T. and K. LePage, 1996: *Development of a Comprehensive Hydroacoustic Coverage Assessment Model*, Air Force Phillips Laboratory Technical Report PL-TR-96-2248, BBN Technical Report No. W1275, Arlington, Va. (UNCLASSIFIED)

Gardner, C., 1993: Gravity Wave Models for the Horizontal Wave Number Spectra of Atmospheric Velocity and Density Fluctuations, *JGR*, 98, D1, 1035-1049. (UNCLASSIFIED)

Gardner, C., 1995: Scale-Independent Diffusive Filtering Theory of Gravity Wave Spectra in the Atmosphere, *The Upper Mesosphere and Lower Thermosphere: A Review of Experiment and Theory*, Geophysical Monograph 87, AGU. (UNCLASSIFIED)

Gibson, R. and D. Norris, 2000: The infrasound analysis tool kit InfraMAP: Capabilities, enhancements and applications, *Proceedings of the 22nd Annual Seismic Research Symposium*, New Orleans, La. (UNCLASSIFIED)

Gibson, R., R. Bieri, and T. Farrell, 1998: *Application of Three-Dimensional Ray Tracing to Infrasonic Propagation in the Atmosphere: The October 1997 El Paso Bolide*, BBN Technical Memorandum No. W1332, Arlington, Va. (UNCLASSIFIED)

Gibson, R. and D. Norris, 2002a: Infrasound propagation modeling: Near-real-time environmental characterization and variability studies, *Infrasound Technology Workshop*, De Bilt, The Netherlands. (UNCLASSIFIED)

Gibson, R. and D. Norris, 2002b: *Development of an Infrasound Propagation Modeling Tool Kit*, Defense Threat Reduction Agency Report DTRA-TR-99-47, Alexandria, Va. (UNCLASSIFIED)

Hedin, A. E, E. L. Fleming, A. H. Manson, F. J. Schmidlin, S. K. Avery, R. R. Clark, S. J. Franke, G. J. Fraser, T. Tsuda, F. Vial, and R. A. Vincent, 1996: Empirical wind model for the upper, middle, and lower atmosphere, *J. Atmos. Terr. Phys.*, **58**, 1421-1447. (UNCLASSIFIED)

Hunter, J. H. and R. W. Whitaker, 1997: Numerical modeling of long range infrasonic propagation, *Infrasound Workshop for CTBT monitoring*, Santa Fe, New Mex. (UNCLASSIFIED)

Jensen, F. B., W. A. Kuperman, M. B. Porter, and H. Schmidt, 1994: *Computational Ocean Acoustics*, AIP Press, New York. (UNCLASSIFIED)

Jones, M. J., J. P. Riley, and T. M. Georges, 1986: *A Versatile Three-Dimensional Hamiltonian Ray-Tracing Program for Acoustic Waves in the Atmosphere above Irregular Terrain*, NOAA Special Report, Wave Propagation Laboratory, Boulder, Co. (UNCLASSIFIED)

Kay, S., 1993: Fundamentals of Statistical Signal Processing: Estimation Theory, Prentice Hall, New Jersey. (UNCLASSIFIED)

McDonald, B. and W. Kuperman, 1987: Time domain formulation for pulse propagation including nonlinear behavior at a caustic, *J. Acoust. Soc. Am.*, **81**, 1406-1417. (UNCLASSIFIED)

McLaughlin, K. L., A. Gault, and D. Brown, 2000: Infrasound detection of rocket launches, *Proceedings of the 22nd Annual Seismic Research Symposium,* New Orleans, Sept. 12-15. (UNCLASSIFIED)

Norris, D. E., J. L. Spiesberger, and D. W. Merdes, 1998: Comparisons of basin-scale acoustic transmissions with rays and further evidence for a structured thermal field in the northeast Pacific, *J. Acoust. Soc. Am.*, **103**, 182-194. (UNCLASSIFIED)

Norris, D. and R. Gibson, and J. Bourdelais, 2001: Infrasonic modeling of recent bolide events using ray and full-wave models, *Superbolide Workshop,* Los Alamos, New Mex. (UNCLASSIFIED)

Norris, D. and R. Gibson, 2001a: InfraMAP propagation modeling enhancements and the study of recent bolide events, *Proceedings of the 23rd Seismic Research Review,* Jackson Hole, Wy. (UNCLASSIFIED)

Norris, D. and R. Gibson, 2001b: InfraMAP propagation modeling enhancements and the study of recent bolide events, *Infrasound Technology Workshop,* Kailua-Kona, Hawaii (UNCLASSIFIED)

Norris, D. and R. Gibson, 2002a: InfraMAP enhancements: Environmental/propagation variability and localization accuracy of infrasonic networks, *Proceedings of the 24th Seismic Research Review,* Ponte Vedra Beach, Fl. (UNCLASSIFIED)

Norris, D. and R. Gibson, 2002b: Propagation variability and localization accuracy of infrasonic networks, *J. Acoust. Soc. Am.*, **112**, No. 5, Pt. 2, 2380. (UNCLASSIFIED)

Norris, D., 2003: *Infrasonic Source Localization*, BBN Technical Memo 1521, BBN Technologies, Arlington, Va. (UNCLASSIFIED)

Norris, D. and R. Gibson, 2003: *User's Guide for InfraMAP Version 3.0*, BBN Technical Report No. W1525, Arlington, Va. (UNCLASSIFIED)

Peitgen, H. and D. Saupe, eds., 1998: *The Science of Fractal Images*, Springer-Verlag. (UNCLASSIFIED)

Perl, R., 1981: *Dependence of localization performance on sensor geometry and measurement accuracy*, BBN Technical Report 4614, BBN Technologies, Cambridge, Mass. (UNCLASSIFIED)

Picone, J. M., A. E. Hedin, S. L. Coffey, J. Lean, D. P. Drob, H. Neal, D. J. Melendez-Alvira, R. R. Meier, and J. T. Mariska, 1997: The Naval Research Laboratory program on empirical models of the neutral upper atmosphere, in *Astrodynamics: Advances in the Astronautical Sciences*, Vol. 97, edited by F. R. Hoots, B. Kaufman, P. J. Cefola, and D. B. Spencer, American Astronautical Society, San Diego, Ca. (UNCLASSIFIED)

Pierce, A. D. and J. W. Posey, 1970: *Theoretical Prediction of Acoustic-Gravity Pressure Waveforms Generated by Large Explosions in the Atmosphere*, Technical Report AFCRL-70-0134, Air Force Cambridge Research Laboratories, Bedford, Mass. (UNCLASSIFIED)

Pierce, A. D., C. A. Moo, and J. W. Posey, 1973: *Generation and Propagation of Infrasonic Waves*, Technical Report AFCRL-TR-73-0135, Air Force Cambridge Research Laboratories, Bedford, Mass. (UNCLASSIFIED)

Pierce, A. D. and W. A. Kinney, 1976: *Computational Techniques for the Study of Infrasound Propagation in the Atmosphere*, Technical Report AFGL-TR-76-56, Air Force Geophysics Laboratories, Hanscom AFB, Mass. (UNCLASSIFIED)

Sutherland, L. C. and H. E. Bass, 1996: Atmospheric absorption in the atmosphere at high altitudes, *Seventh Symposium on Long Range Sound Propagation*, Ecole Centrale de Lyon, France. (UNCLASSIFIED)

Tenney, S. and J. Noble, 2000: Multiple infrasonic arrays in an urban environment (U), *Meeting of the MSS Specialty Group on Battlefield Acoustics and Seismics*, Laurel, MD, Oct 17-19. (UNCLASSIFIED)

West, M., K. E. Gilbert, and R. A. Sack, 1992: A tutorial on the Parabolic Equation (PE) model used for long range sound propagation in the atmosphere, *Applied Acoustics*, **37**, 31-49. (UNCLASSIFIED)

Pierce, A. D., C. A. Moo, and J. W. Posey, 1973: *Generation and Propagation of Infrasonic Waves*, Technical Report AFCRL-TR-73-0135, Air Force Cambridge Research Laboratories, Bedford, Mass. (UNCLASSIFIED)

Pierce, A. D. and W. A. Kinney, 1976: *Computational Techniques for the Study of Infrasound Propagation in the Atmosphere*, Technical Report AFGL-TR-76-56, Air Force Geophysics Laboratories, Hanscom AFB, Mass. (UNCLASSIFIED)

Appendix
Abbreviations and Acronyms

AFTAC	Air Force Technical Applications Center
AGU	American Geophysical Union
CTBT	Comprehensive Nuclear Test Ban Treaty
GUI	Graphical User Interface
HARPA	Hamiltonian Ray-Tracing Program for Acoustic Waves in the Atmosphere
HWM	Horizontal Wind Model
IMS	International Monitoring System
InfraMAP	Infrasonic Modeling of Atmospheric Propagation
LANL	Los Alamos National Laboratory
MSIS or MSISE	Extended Mass Spectrometer - Incoherent Scatter Radar model
NASA	National Aeronautics and Space Administration
NOAA	National Oceanographic and Atmospheric Administration
NPE	Nonlinear Progression Wave Equation
NRL	Naval Research Laboratory
PE	Parabolic Equation
TDPE	Time Domain Parabolic Equation
TXIAR	Texas Infrasound Array
UT	Universal Time
WKB	Wentzel-Kramer-Brillouin method

DEPARTMENT OF DEFENSE

DEFENSE TECHNICAL
INFORMATION CENTER
8725 JOHN J. KINGMAN ROAD,
SUITE 0944
FT. BELVOIR, VA 22060-6201
2 CYS ATTN: DTIC/OCA

ITT INDUSTRIES
ITT SYSTEMS CORPORATION
1680 TEXAS STREET, SE
KIRTLAND AFB, NM 87117-5669
2 CYS ATTN: DTRIAC

DEPARTMENT OF DEFENSE CONTRACTORS

BBN TECHNOLOGIES
1300 NORTH 17TH STREET
SUITE 400
ARLINGTON, VA 22209
ATTN: D. NORRIS